

1
2
3
4
5
6
7
8
9
10
11
12
13
14
15
16
17
18
19
20
21
22
23
24
25
26
27
28
29
30
31
32
33
34
35
36
37
38
39
40
41
42
43
44
45
46
47
48
49
50
51
52
53
54
55
56
57
58
59
60
61
62
63
64
65

Insights into the atypical autokinase activity of the *Pseudomonas aeruginosa* GacS histidine kinase and its interaction with RetS

Firas Fadel^{¶1§}, Violla Bassim^{¶1∅}, Vanessa I. Francis², Steven L. Porter², Thomas Botzanowski⁴, Pierre Legrand³, Maria Maté Perez¹, Yves Bourne¹, Sarah Cianférani⁴, Florence Vincent^{1,5*}

¹ CNRS, Aix Marseille Université, AFMB, Marseille, France

² Biosciences, College of Life and Environmental Sciences, University of Exeter, Exeter, United Kingdom

³ Synchrotron SOLEIL, L'Orme des Merisiers, Gif-sur-Yvette, France.

⁴ Laboratoire de Spectrométrie de Masse BioOrganique, Université de Strasbourg, CNRS, IPHC UMR 7178, Strasbourg, France

[§] Present address: Biozentrum University of Basel, Basel, Switzerland

[∅] Present adress : CNRS, Institut Curie, Paris, France

[¶] These authors contributed equally to the work

⁵ Lead contact

*Correspondence should be addressed to Florence Vincent

email: fvincent.cnrs@univ-amu.fr

Keywords

Histidine kinase, *Pseudomonas aeruginosa*, GacS, RetS, structure, autokinase activity, protein-protein interactions

Abstract

Virulence in *Pseudomonas aeruginosa* (PA) depends on complex regulatory networks, involving phosphorelay systems based on two-component systems (TCSs). The GacS/GacA TCS is a master regulator of biofilm formation, swarming motility and virulence. GacS is a membrane-associated unorthodox histidine kinase (HK) whose phosphorelay signaling pathway is inhibited by the RetS hybrid HK. Here we provide structural and functional insights into the interaction of GacS with RetS. The structure of the GacS HAMP-H1 cytoplasmic regions reveals an unusually elongated homodimer marked by a 135 Å long helical bundle formed by the HAMP, the signaling helix (S-helix) and the DHp subdomain. The HAMP and S-helix regions are essential for GacS signaling and contribute to the GacS/RetS binding interface. The structure of the GacS D1 domain together with the discovery of an unidentified functional ND domain, essential for GacS full autokinase activity, unveils signature motifs in GacS required for its atypical autokinase mechanism.

Main Text

Introduction

Pseudomonas aeruginosa (PA) is a major opportunistic pathogen that has developed genetic traits to thrive in various natural habitats and infect plants, animals, and insects with an important arsenal of virulence factors. In the last decades, PA has become a major human pathogen as it causes nosocomial infections worldwide and severe infections in patients with cystic fibrosis, hospitalized with cancer, severely burned or in intensive care units (Nathwani et al., 2014; Winstanley et al., 2016). PA can cause acute or chronic infections, and the choice between these two infection modes depends on the ability of PA to switch from a planktonic (free-swimming) to a sedentary (biofilm) lifestyle, the latter being difficult to eradicate due to the antibiotic-resistant nature of its biofilm (Micek et al., 2015; Sousa and Pereira, 2014). In PA, the acute-to-chronic transition is regulated by complex regulatory networks involving two-component regulatory systems (TCS).

TCSs are widespread in bacteria. They sense and transduce environmental signals into appropriate cellular responses to contribute to bacterial survival, cellular development, and pathogenicity (Zschiedrich et al., 2016). TCSs are composed of a histidine kinase (HK) and a response regulator (RR), two proteins that function together through a phosphorelay mechanism, which functions mainly as a two-step mechanism. First, detection of a stimulus by the periplasmic domain (for

1 transmembrane HKs) triggers HK autophosphorylation on a conserved histidine (H) residue from
2 the transmitter H1 domain. The H1 domain comprises two separate sub-domains: a DHp domain
3 containing the conserved His residue and an ATP-binding kinase domain (CA). The HKs function
4 as dimers and each monomer's ATPase activity catalyzes the trans or cis-phosphorylation reaction
5 of the histidine residues (Ashenberg et al., 2013; Casino et al., 2010). In a second step, the
6 phosphoryl group on the H1 domain is transferred onto a conserved aspartate (D) residue present
7 in the receiver or D domain of the cognate response regulator (RR) (Jacob-Dubuisson et al., 2018;
8 Stock et al., 2000). Alternatively, HKs can possess additional cytoplasmic domains such as a
9 second receiver domain (D1) often fused to the HK or an alternative histidine-phosphotransfer
10 domain (Hpt or H2) which can be either fused to the HK (H2) or forms a third independent
11 component named Hpt protein. HK carrying two additional D1 and H2 domains are called
12 unorthodox HKs (unorthoHKs) while those carrying only a D1 domain are called hybrid HK
13 (hybHK) (Stock et al., 2000).

23 In PA, the GacS/GacA phosphorelay system is a master regulator for transitioning from acute
24 to chronic infection (Gao and Stock, 2010). The complex architecture of the GacS unorthoHK
25 comprises an N-terminal transmembrane α -helix followed by a periplasmic sensor domain
26 (GacS_{PD}) and tailed with a second transmembrane α -helix, linked to four cytoplasmic domains,
27 the HAMP (HK, Adenylyl cyclase, Methyl binding protein, Phosphatase) domain, the transmitter
28 H1 domain made of the DHp (Dimerization and Histidine phosphotransfer) and the catalytic (CA)
29 subdomains, a receiver (D1) domain and completed by a histidine-phosphotransfer (H2) domain
30 (Heeb and Haas, 2001) (Figure 1A). Upon recognition of a yet unknown signal by GacS_{PD},
31 conformational changes should propagate through the two transmembrane helices and transduce
32 to the cytoplasmic region via the HAMP domain (Ali-Ahmad et al., 2017; Lapouge et al., 2008;
33 Zuber et al., 2003). These putative structural rearrangements initiate the presumably H1 trans-
34 phosphorylation to trigger a four-step phosphorelay from the H1 to the D1 conserved aspartate,
35 then to the H2 conserved histidine (Figure 1A), and finally to a conserved aspartate on the GacA
36 RR. Once phosphorylated, GacA activates the expression of the two small non-coding RNAs,
37 RsmY and RsmZ. These RNAs titrate the translational regulator RsmA, which upregulates genes
38 involved in biofilm formation, including those coding for major exopolysaccharides (EPSs) and
39 Type 6 Secretion System (T6SS) while downregulating those required for acute infection such as
40 swarming motility and Type 3 secretion (Workentine et al., 2009; Gooderham and Hancock,
41 2009).

58 The GacS/GacA TCS is activated during the early stages of biofilm formation, and induces
59 chronic infections by down-regulating genes involved in acute infection. Therefore, the
60

1 GacS/GacA signalling network has received great attention to document the key molecular
2 mechanisms of this decision-making machinery (Kitten et al., 1998; Lapouge et al., 2008). The
3 GacS/GacA TCS is at the centre of a multikinase signalling network for which three hybrid
4 sensors HKs, named LadS, RetS and PA1611, act in concert to either promote GacS signalling to
5 favour biofilm formation in chronic infection or to impede GacS signaling to favor production of
6 virulence factors in acute infection (Bhagirath et al., 2017; Ventre et al., 2006). In this pathway,
7 RetS inhibits the GacS signalling. RetS is an orphan membrane hybHK devoid of a cognate RR,
8 and its cytoplasmic region consists of an H1 domain, made of the DHp and a degenerated CA
9 subdomains unable to autophosphorylate (Mancl et al., 2019), followed by two receiver D1 and
10 D2 domains (Figure 1A). RetS HK uses three mechanisms to interfere with GacS signalling. First,
11 the RetS_{D2} domain can act as a phosphatase on GacS_{H1}; second, the RetS_{H1} domain has a
12 transmitter phosphatase activity against the GacS_{D1} domain (Francis et al., 2018), and third, RetS
13 uses direct interactions through the respective DHp subdomains of the two HKs, to impede GacS
14 signaling (Mancl et al., 2019; Ryan Kaler et al., 2021). Upon RetS inhibitory activity, the level of
15 the two small RNAs RsmY and RsmZ is reduced, preventing biofilm formation, which
16 concomitantly enhances acute infection.

17
18
19
20
21
22
23
24
25
26
27
28
29 Despite a general understanding of the GacS/GacA signaling pathway, it remains elusive
30 how GacS regulates its autokinase and phosphorelay mechanisms to trigger the acute/chronic
31 switch. Herein, we solved the crystal structures of GacS_{HH1} (construct a.a 220 to 512), which spans
32 from the second helix of the HAMP domain to the end of the H1 domain and the isolated GacS_{D1}
33 domain at 2.65 Å and 1.9 Å resolution, respectively. The GacS_{HH1} structure shows a remarkable
34 rod shape due a 135 Å long continuous N-terminal helix, linking the HAMP domain to the DHp
35 through a signaling helix (S-helix). The HAMP/S-helix region is essential for modulating GacS
36 signal transduction, as revealed by *in vitro* studies and *an in vivo* infection model using
37 chromosomal *gacS* variants. Moreover, the weak autokinase activity of the GacS_{HH1} domain
38 compared to that of the entire GacS cytoplasmic region (GacS_{CytoFL}) allowed us to identify an
39 unusual conformation of the ATP lid motif in the CA domain that is not observed in other related
40 HKs. Most importantly, a yet uncharacterized domain (ND), inserted between the CA and the D1
41 domains, is essential to restore a full GacS autokinase activity. Structural comparison between
42 GacS and other characterized unorthodox and hybrid HKs harboring ND-like domains, together
43 with a structural analysis of the isolated D1 domain, provides insights into the arrangement of the
44 GacS cytoplasmic multiple domains necessary for its autokinase and phosphor-signaling
45 activities. Finally, size exclusion chromatography coupled to native MS (SEC-nativeMS) analysis
46 reveals the formation of a 1:1 stoichiometric RetS:GacS assembly and highlights the importance
47
48
49
50
51
52
53
54
55
56
57
58
59
60
61
62
63
64
65

1
2
3
4
5
6
7
8
9
10
11
12
13
14
15
16
17
18
19
20
21
22
23
24
25
26
27
28
29
30
31
32
33
34
35
36
37
38
39
40
41
42
43
44
45
46
47
48
49
50
51
52
53
54
55
56
57
58
59
60
61
62
63
64
65

of the GacS HAMP region at the binding interface. Altogether, our results show an atypical autokinase activity in GacS and reveal specific interactions with RetS, which are essential to the decision-making process during PA infection.

Results

The GacS_{H1} structure shows an elongated coiled-coil

The 2.65 Å GacS_{H1} structure (construct a.a. 220 to 512) shows an elongated, 135 Å long, shape which delineates two main regions, a long helical segment that spans the HAMP α 2 helix to the α 3 helix of the DHp domain, and the 4 α /5 β domain corresponding to the canonical ATP kinase/CA domain (Figures 1B and S1A). The sub-helices connecting the HAMP and DHp define a signaling helix motif (S-helix) that integrates into the long helical structure. As for many HKs, the GacS_{H1} structure adopts a homodimeric arrangement, as observed in solution by SEC-native MS analysis (Figure S2A), made of a central extended coiled-coil flanked on each side by the two CA domains (Figure 1B). The dimeric interface, which spans residues from the S-helix and the DHp domain (Figure 1B, 2B, and C), has a large buried surface (~2200 Å² on each subunit) dominated by hydrophobic residues (Figure 2B and 2C). Such a biologically relevant elongated coiled-coil arrangement highlights a large distance occurring between the cytoplasmic membrane and the GacS H1 domain, as observed for the related VicK and NarQ HKs (Gushchin et al., 2017; Wang et al., 2013). The GacS_{H1} CA domain (residue 355 to 511) shows a typical α/β sandwich fold with four helices packed against five anti-parallel β strands, as typically observed in other HKs and exemplified by an rmsd of 1.6 Å over 132 C α residues when compared to the corresponding CA domain of HK853 (PDB: 4JAU) (Figure 1B and S3 and S4) (Podgornaia et al., 2013). Moreover, the conserved nucleotide-binding sequences, which comprise critical residues in the N, G1, G2, and F boxes within the ATP binding site, are conserved in GacS (Kim and Forst, 2001) (Figure S3A). The DHp region shows a canonical four-helix bundle exhibiting a right-handed arrangement, in which the CA domain of one subunit can transphosphorylate the catalytic histidine on the adjacent subunit, which confirms the data obtained for GacS transphosphorylation (Ryan Kaler et al., 2021) (Figure 1B, S4). Therefore, the GacS CA domain adopts an open symmetric conformation away from the phosphorylatable H293 on the adjacent monomer (Figure 1B, S4). This is consistent with an inactive HK form, as reported for the WalK HK structure, and it is supported by the absence of a bound ATP molecule in the GacS structure, even from crystals grew in presence of ATP (data not shown) (Cai et al., 2017).

In addition to the GacS_{H1} structure, we solved the structures of the isolated GacS_{D1} in the absence or presence of the BeF₃⁻ phosphate analog. GacS_{D1} adopts the classical ($\beta\alpha$)₅ CheY fold

1
2
3
4
5
6
7
8
9
10
11
12
13
14
15
16
17
18
19
20
21
22
23
24
25
26
27
28
29
30
31
32
33
34
35
36
37
38
39
40
41
42
43
44
45
46
47
48
49
50
51
52
53
54
55
56
57
58
59
60
61
62
63
64
65

reminiscent of the OmpR/PhoB-type response regulators (Nguyen et al., 2015). The BeF₃-bound GacS_{DI} structure confirms the conserved D715 to act as the phosphor-acceptor in GacS HK (Bourret, 2010) (Figure 1C).

A S-helix region is embedded in the coiled coil

The GacS_{HHI} structure contains the $\alpha 2$ helix preceded by a 3-residue extension belonging to the $\alpha 1$ - $\alpha 2$ connector of the HAMP domain (Figure 1B and 2B). Crystal packing analysis indicates that the $\alpha 2$ helix pair from an adjacent subunit in the crystal, mimics a four-helix bundle that stabilize the N-terminal region of the structure (Figure S5). In addition to the HAMP domain, the GacS_{HHI} structure unveils a 40-residue helical segment (aa 240-274) that corresponds to a signaling helix (S-helix). This module, which was misannotated in GacS, is often observed between two signaling domains in other HKs (Anantharaman et al., 2006; Stewart and Chen, 2010). The S-helix forms a parallel coiled-coil at the dimeric interface and merges contiguously between the HAMP- $\alpha 2$ and the DHp- $\alpha 3$ helices (Figure 1B, 2A, B). The HAMP, S-helix, and DHp modules display heptad repeats periodicity, in which the inner heptad a and d positions are occupied by hydrophobic residues (McLachlan and Stewart, 1975). Noteworthy, two polar residues N259 and Q266 are found at position d in two consecutive heptads in the middle of the S-helix (Figure 2A, C). These polar residues establish a hydrogen bond with their cognate residues in the adjacent monomer (Figure 2C), a feature known to destabilize a coil-coil (Thomas et al., 2017). A detailed structural analysis shows a local increase of the coiled-coil radius near the 238-241 segment at the end of the HAMP- $\alpha 2$ helix, corresponding to a stutter region at position L238 (referred as a/d residue in Stewart & Chen 2010 (Stewart and Chen, 2010)) (Figures 2D and S6). This discontinuity, widely conserved in the other BarA, NarX, and NarQ HKs, characterizes the hinge region between the HAMP domain and the S-helix (Stewart and Chen, 2010; Zhou et al., 2009) (Figure 2A, D). Following the same nomenclature, the GacS S-helix is composed of 6 heptad repeats with the first S1 heptad repeat located within the HAMP- $\alpha 2$ helix to form the stutter. However, the ERT signature in the S3 heptad, which is conserved among S-helices, is not conserved in GacS as observed for BarA where an A residue occupies position d instead of an R or K (Stewart and Chen, 2010) (Figure 2D).

The HAMP and the S-helix domains are regulatory elements of GacS autokinase activity

To ascertain the functional role of the two helical HAMP and S-helix regions in GacS, we engineered a PAO1 derivative (GacS $\Delta 76$) with a chromosomal mutation, in which the region encoding the 79 residues (S190 to I269) that comprises the HAMP and most of the S-helix region

1 was replaced with a sequence encoding a 3-residue linker (EAF) (Figure S1A), as previously
2 performed in *P. fluorescens* (Zuber et al., 2003).

3
4 As the GacS network plays a major role in regulating exopolysacchide production
5 (associated with biofilm formation and chronic infection) and swarming motility (associated with
6 acute infection), behavior of the GacS $_{\Delta 76}$ strain was compared with the wild-type strain (PAO1),
7 the *gacS* deletion strain ($\Delta gacS$), and the *retS* deletion strain ($\Delta retS$) using i) swarming assays,
8 and ii) Congo Red plates to gauge exopolysaccharide production and motility. In the swarming
9 assays, the PAO1 and $\Delta gacS$ strains formed large swarms, whereas the $\Delta retS$ and GacS $_{\Delta 76}$ strains
10 did not swarm and instead remained at the inoculation point (Figure 3A). The lack of swarming
11 in the $\Delta retS$ strain is due to high levels of GacS activity as GacS is unconstrained by RetS in this
12 mutant (Francis et al., 2018). Consistent with this explanation, a $\Delta retS \Delta gacS$ double mutant can
13 swarm albeit at slightly reduced levels compared to PAO1. (Figure 3B). The similarity in
14 phenotype between the $\Delta retS$ and *gacS* $_{\Delta 76}$ strains supports the hypothesis that like the $\Delta retS$ strain,
15 GacS activity is elevated in the *gacS* $_{\Delta 76}$ mutant. This observation is confirmed on Congo Red
16 plates (Figure 3E), where the *gacS* $_{\Delta 76}$ mutant behaved like the $\Delta retS$ mutant, forming smaller
17 denser colonies than the PAO1 strain, suggesting they both have increased GacS activity.

18
19 To assess the effect of the loss of HAMP and S-helical regions on GacS virulence, we
20 used *Galleria mellonella* larvae as an infection model. The larvae were infected with 20 to 40
21 CFUs of the *gacS* $_{\Delta 76}$, $\Delta gacS$, $\Delta retS$, and PAO1 strains. Infection with the PAO1 and $\Delta gacS$ strains
22 caused all the larvae to die within 20 hours of infection, while the $\Delta retS$ mutant showed greatly
23 reduced lethality with more than 70% of larvae surviving after 76h. The *gacS* $_{\Delta 76}$ mutant showed
24 a similarly reduced virulence phenotype as the $\Delta retS$ mutant (Figure 4), which is consistent with
25 GacS $_{\Delta 76}$ being hyperactive.

26
27 Altogether, we show that the *gacS* $_{\Delta 76}$ mutant functions as if RetS was inactive and unable
28 to inhibit GacS $_{\Delta 76}$ i.e. the *gacS* $_{\Delta 76}$ mutant phenocopies the *retS* deletion mutant. This could mean
29 that the constitutively active *gacS* $_{\Delta 76}$ mutant is resistant to the inhibitory effects of RetS due to the
30 loss of an interacting region, or it may simply overwhelm the inhibitory effects of RetS.

31 **The GacS-HAMP domain is involved in the formation of the GacS:RetS complex**

32
33 We next investigated a possible implication of these two HAMP/S-helix helical regions in
34 a direct interaction with RetS. This hypothesis is driven by a topological comparison of the GacS
35 and RetS models anchored to the internal membrane that reveals a significant, 90 Å, shift in the
36 position of the DHp domains due to the absence of the HAMP and S-helix domains in RetS
37 (Figure 5). To characterize the GacS/RetS interaction and their oligomerization states in solution,
38
39
40
41
42
43
44
45
46
47
48
49
50
51
52
53
54
55
56
57
58
59
60
61
62
63
64
65

1 we performed online SEC-native MS experiments. We thus compared the interaction behavior
2 between RetS_{HI} and each of the three GacS_{CytoFL}, GacS₂₅₂₋₉₂₅ and GacS_{HHI} cytoplasmic constructs
3 (Figure S1). The GacS₂₅₂₋₉₂₅ construct lacks the HAMP and part of the S-Helix region. Online
4 SEC-native MS analysis revealed three major peaks for all equimolar mixtures of the GacS
5 variants and RetS_{HI} (Figure 6): the most intense one (labelled 2, 4 or 6 depicted in Figure 6 A-C
6 respectively) corresponds to GacS homodimers with measured molecular masses ranging from 60
7 to 160 kDa depending on the variant (Figure 6G, S2), followed by a second one (labelled 3, 5 or
8 7 depicted in Figure 6 A-C respectively) of varying intensity with masses from 59 to 107 kDa in
9 agreement with a 1:1 stoichiometric GacS:RetS complex (Figure 6 D-F, S7). The third one, at ~
10 8 min (labelled 1, Figure 6A) corresponds to the RetS_{HI} homodimer (55 kDa, Figure 6G and S2B).

11 In line with SEC-native MS data, and to evaluate the role of the HAMP and S-Helix region
12 in the interaction with RetS, we performed microscale thermophoresis (MST) assays using RetS_{HI}
13 and three GacS variants (Figure S1). For the different GacS:RetS_{HI} complexes, we measure
14 dissociation constants of $K_d=41\pm 25$ nM and 71 ± 36 nM for GacS_{CytoFL} and GacS_{HHI}. These values
15 are in agreement with the K_d value of 33 nM reported for the GacS_{HHI} and RetS_{HI} complex
16 (Goodman et al., 2009). However, for the two constructs missing the HAMP and S-helix regions,
17 we obtain K_d values of 433 ± 170 nM for GacS₂₅₂₋₉₂₅ and 832 ± 250 nM for GacS₂₈₀₋₉₂₅ (Figure 7A),
18 indicating the implication of the HAMP domain in the GacS:RetS binding interface. Moreover,
19 the K_d values in the μ M range for GacS₂₅₂₋₉₂₅ and GacS₂₈₀₋₉₂₅ variants indicate that weaker
20 interactions occur in the GacS:RetS complex, e.g. between RetS_{HI} and GacS_{DI}, as RetS_{HI} can
21 dephosphorylate GacS_{DI} (Francis et al., 2018). However, no definitive conclusions could be
22 reached for the implication of the S-helix region in the interfacial region, as similar K_d values are
23 observed for the two truncated GacS₂₅₂₋₉₂₅ and GacS₂₈₀₋₉₂₅ variants. A previous study showed the
24 GacS:RetS complex as heterodimers of GacS and RetS homodimers (Mancl et al., 2019). In this
25 study, we did not observe higher oligomeric forms besides the 1:1 stoichiometry using the SEC-
26 MS approach. However, our SEC-native MS data are consistent with a recent study that reports
27 homodimers disruption upon heterodimer formation between RetS_{HI} and GacS-DHp domain
28 (Ryan Kaler et al., 2021).

29 Overall, these results demonstrate that a GacS:RetS complex disassembles the
30 homodimeric form required for GacS activity, and unveils the important role of the HAMP
31 domain for the GacS:RetS binding interface.

32 **The unusual weak autokinase activity of the GacS CA domain**

1 We next investigated the catalytic properties of different GacS constructs using
2 radiolabeled $\gamma^{32}\text{P}$ ATP. Unexpectedly, almost no autokinase activity could be observed for the
3 GacS_{HH1} construct (Figure 8A, panel 1) compared to the GacS_{CytoFL} construct harboring all
4 cytoplasmic domains (Figure 8A, panel 2). This is surprising as the presence of conventional DHP
5 and CA domains appears sufficient to confer a significant autophosphorylation activity in other
6 HKs (Casino et al., 2014). A GacS₁₉₀₋₅₁₂ variant harbouring a complete HAMP domain showed a
7 similar loss of activity (Figure 8A, panel 3), arguing that an incomplete HAMP domain in GacS_{HH1}
8 is not responsible for the lack of autokinase activity. Although the structure of the GacS CA
9 domain is devoid of a bound nucleotide, it reveals an unusual 19-residue helix (449-468) in the F
10 box fused to a structured helical ATP lid. To assess the ability of the GacS CA domain to bind
11 ATP, we determine the K_d value between GacS_{HH1} and the ATP analog, adenosine 5'-[β , γ -
12 imido]triphosphate (AMPPNP) by MST. The measured K_d value of $2.5 \pm 1.8 \mu\text{M}$ is closely similar
13 to those previously reported for classical HKs using AMPPNP (Bhate et al., 2015) (Figure 7B),
14 suggesting that the atypical helical ATP lid in GacS could undergo conformational changes to
15 accommodate ATP. To check the role of the atypical ATP lid in the inactive conformation of the
16 GacS catalytic core, we generated a chimera by replacing the GacS ATP lid region (Q461-Q469)
17 with the corresponding R430-E438 motif from the HK853, which is known to show a high
18 autophosphorylation rate (Marina et al., 2005) (Figure S3C). Interestingly, the GacS chimera did
19 not recover a full phosphorylation rate even after a 60 min incubation time with $\gamma^{32}\text{P}$ -ATP as
20 observed for GacS_{HH1} at this time point (Figure 8B).

21 In contrast to classical HKs with the conventional topology of the DHP and CA modules, the
22 autokinase activity of the unorthodox GacS HK may have other levels of regulation. These results
23 point to a possible participation of other GacS cytoplasmic regions downstream the CA domain,
24 to trigger autokinase activity.

25 **An uncharacterized pseudoreceiver domain is essential for GacS autokinase activity**

26 To understand the molecular basis for the lack of autokinase activity of GacS_{HH1} relative
27 to the normal activity of GacS_{CytoFL}, we conducted a bioinformatic analysis of the entire GacS
28 sequence that revealed an unannotated 150-residue cytoplasmic domain (524 to 638), denoted ND
29 domain, inserted between the CA and D1 domains (Figure S8A). To check whether this
30 uncharacterized ND domain could be involved in the GacS autokinase activity, we generated the
31 GacS_{HH1ND} construct comprising the HH1 region followed by the ND domain (Figure S1A).
32 Surprisingly, the GacS_{HH1ND} variant restores the autokinase activity to a slightly higher level than
33 that of GacS_{CytoFL}, mainly due to its incapacity to perform the concomitant phosphatase activity

1
2
3
4
5
6
7
8
9
10
11
12
13
14
15
16
17
18
19
20
21
22
23
24
25
26
27
28
29
30
31
32
33
34
35
36
37
38
39
40
41
42
43
44
45
46
47
48
49
50
51
52
53
54
55
56
57
58
59
60
61
62
63
64
65

carried out by the D1 domain (Figure 8A, panel 4). A competition-based activity assay of GacS_{HH1ND} between $\gamma^{32}\text{P}$ -ATP and cold ATP yields a K_m value of 92.66 μM , which is in the similar 10 to 200 μM range observed for other HKs (Bhate et al., 2015), and a K_{cat} value of 1.17 s^{-1} (Figure 8C). To confirm the functional role of the ND domain in the GacS autokinase activity, we generated the GacS_{CytoFL} construct lacking the ND domain (GacS_{CytoFL Δ ND}, Figure S1A). Consistent with the activity of GacS_{HH1ND}, deletion of ND reveals a pronounced impact, with a residual activity of only 5% compared to the GacS_{CytoFL} activity (Figure 8A panel 2, and 8B). Moreover, the obtained K_d value of $3.2 \pm 1.5 \mu\text{M}$ between GacS_{HH1ND} and AMPPNP is closely similar to that observed with GacS_{HH1} (2.5 μM), suggesting that ND is not involved in ATP binding (Figure 7B).

To test the role of the ND domain *in vivo*, we generated chromosomal in-frame deletion mutants where the ND sequence was removed; these were created in both wild-type (PAO1 strain) and $\Delta retS$ strain backgrounds. We phenotypically characterized these mutants using Congo red plates and swarming assays where we compared their behavior with control strains: PAO1 (wild-type), $\Delta gacS$ (in frame deletion of the entire *gacS* gene), and *gacS*(N410D) (a chromosomal point mutant where GacS autophosphorylation has been disabled by mutating an N-box residue (N410) that is critical for autophosphorylation) (Dutta and Inouye, 1996) - N347D of EnvZ corresponds to N410D of GacS; Francis and Porter, unpublished for experimental verification that purified GacS(N410D) lacks kinase activity). From the Congo red plates, the $\Delta gacS$, *gacS* Δ ND and, *gacS*(N410D) point mutant all formed larger colonies than PAO1 (Figure 3F, and G). Significantly, the double mutants, $\Delta retS \Delta gacS$, $\Delta retS gacS \Delta$ ND and $\Delta retS gacS$ (N410D), all gave larger colonies than PAO1 (Figure 3F, and G), suggesting that these *gacS* mutants suppress the small colony phenotype typically observed with the $\Delta retS$ mutant. The identical behaviors of the $\Delta gacS$, *gacS* Δ ND and *gacS*(N410D) mutants are consistent with a loss of GacS function. From the swarming plates, the *gacS* Δ ND, *gacS*(N410D) and $\Delta gacS$ mutants are capable of swarming at levels similar to PAO1, while a $\Delta retS$ mutant is unable to swarm and remains at the inoculation point (Figure 3A and D). These three mutants are able to suppress the $\Delta retS$ phenotype as the double mutants restore swarming (Figure 3B and C). Again, this is consistent with a loss of GacS autokinase activity in *gacS* Δ ND, *gacS*(N410D) and $\Delta gacS$.

Altogether, these assays confirm that the ND domain is essential for GacS activity and point to an atypical regulatory mechanism of the GacS autokinase activity.

The role of the ND and D1 domains in GacS autokinase activity

1
2
3
4
5
6
7
8
9
10
11
12
13
14
15
16
17
18
19
20
21
22
23
24
25
26
27
28
A BLAST search using the ND domain sequence revealed that this domain is not exclusive to GacS but is present in a wide range of unorthodox HKs among *Pseudomonas* species and also in other Gram-negative bacteria like *Escherichia Coli* with BarA unHK (23% id.), RcsC hybHK (19% id.) and the *Caulobacter crescentus* ShkA unorthoHK (17% id). Recently, the structures of the ShkA and RcsC HKs revealed that their corresponding ND domains consist of a CheY-like fold, as we could predict for GacS ND, and behave as pseudoreceiver domains (PRD) (Dubey et al., 2019; Rogov et al., 2006) (Figure S8B). RcsC is a membrane HK that autophosphorylates using its RcsC-ABL (equivalent to ND) domain, although no function has been yet assigned to this domain. On the other hand, ShkA is in an autoinhibited state. ShkA becomes active only when its Rec1 (equivalent to GacS ND) binds to c-di-GMP by competing with a conserved DDR motif located in the Rec1-Rec2 linker and closely tethering Rec2 (equivalent to GacS D1) interaction. Binding of c-di-GMP displaces the Rec2 domain, leading to an active open state conformation (Dubey et al., 2019). Of note, ShkA residues involved in c-di-GMP binding and in the Rec1-Rec2 linker are not conserved in GacS, suggesting that GacS ND is not able to bind c-di-GMP and residues within the ND-D1 linker have different chemical properties (Figure S8 C, D).

29
30
31
32
33
34
35
36
37
38
39
40
41
42
43
44
45
46
47
48
49
50
51
52
53
54
55
56
57
58
59
60
61
62
63
64
65
In the GacS HK, the GacS_{D1} domain is a receiver domain positioned downstream the ND domain. As the ND domain does not exhibit any conserved aspartate residue, we assume that the GacS_{D1} phosphatase activity transfers phosphate from H293 to its phosphorylatable D715, as observed in the BeF₃⁻-bound GacS_{D1} structure (Figure 1C). Such phosphorelay event is observed in the GacS_{cytoFL} phosphorylation assays, showing a decrease in the phosphorylation rate at 120 min due to the GacS_{D1} phosphatase action, which is suppressed in GacS_{HHIND} lacking the D1 domain (Figure 8A, panel 2 and 4). Following the concept that GacS and ShkA would not follow similar conformational changes to trigger autophosphorylation and phosphotransfer events, we compared GacS_{D1} with the corresponding ShkA Rec2 domain (Figure S9 A and B). An overlay of the two domains reveals an extended helix α_3 in GacS_{D1} compared to a shorter helix α_3 in ShkA-Rec2 (Figure S9A). ShkA uses the tip of helix α_3 to tether Rec2 on the DHp subdomain to lock an inactive state (Figure S9C). When superimposing GacS_{D1} on ShkA Rec2, we observe that a 5-residue insertion (732-736) in the GacS_{D1} helix α_3 creates a steric hindrance that prevents GacS_{D1} to adopt a similar buried position as observed for Rec2 in ShkA (Figure S9A and B). Unlike the autoinhibited closed conformation of ShkA, it is noteworthy that GacS_{cytoFL} adopts a conformation that allows autophosphorylation and phosphotransfer. Taken together, we expect motions of the GacS cytoplasmic domains to adopt a released conformation to confer the autokinase and phosphotransfer activities.

Discussion

1
2
3
4
5
6
7
8
9
10
11
12
13
14
15
16
17
18
19
20
21
22
23
24
25
26
27
28
29
30
31
32
33
34
35
36
37
38
39
40
41
42
43
44
45
46
47
48
49
50
51
52
53
54
55
56
57
58
59
60
61
62
63
64
65

The GacS unorthoHK, which belongs to the class I kinase family (Bilwes et al., 1999), is one of the most complex transmembrane HK in bacteria with six functional domains and is over 100 kDa in size. The structure of the GacS_{HH1} homodimer has provided key structural features marked by an elongated coiled-coil that comprises the HAMP, S-helix, and DHP domains. Although we could not document the structure of the entire HAMP domain, it is reasonable to predict that it forms a four-helix bundle at the C-terminus of the second transmembrane helix. The S-helix module acts as a signal- transduction element and undergoes segmental movements to propagate conformational changes over long distances (Anantharaman et al., 2006; Saita et al., 2015). In this context, it was reported for other HKs that stabilization of the S-helix favours formation of the phosphatase state, preventing autokinase activity, while S-helix destabilization triggered by conformational rearrangements of the HAMP four-helix bundle induces autophosphorylation (Saita et al., 2015)(Gushchin et al., 2017). Therefore, sensing of an environmental signal by the GacS periplasmic domain should trigger primary helical movements along the two transmembrane helices that will propagate through the HAMP helix bundle, and be transmitted to the catalytic core via the S-helix.

Chromosomal deletion of the HAMP-S-helix region (GacS_{Δ76}) leads to an increase of GacS/GacA activity, arguing for a loss of cooperativity between the HAMP and the S-helix to control GacS signaling events. The phenotype of *gacS*_{Δ76} mutant is similar to a *ΔretS* mutant which suggests either that GacS is not subjected to the three inhibitory mechanisms of RetS hybHK when its HAMP-S-helix segment is deleted, even though all GacS domains required for crosstalk with RetS are present and functional (Francis et al., 2018), or that GacS_{Δ76} activity is so high that the three inhibitory mechanisms are overwhelmed. In the GacS/RetS interaction analysis, an *in vivo* study showed that a heterodimeric DHP interfacial mutant (GacS_{I302V}) that reduced RetS binding, produced a hyperbiofilm phenotype comparable to a *ΔretS* mutant (Ryan Kaler et al., 2021). Therefore, a mutation in GacS preventing or reducing its interaction with RetS should lead to a hyperbiofilm phenotype, suggesting that the disruption of the binding interface between GacS-HAMP region and RetS_{HH1} could be responsible for an enhanced GacS activity phenotype. This is in agreement with the binding constants obtained for the GacS₂₅₂₋₉₂₅ and GacS₂₈₀₋₉₂₅ constructs which are 10 times lower than the values obtained for the constructs containing the HAMP region (Figure 7A). Moreover, one can argue that this crosstalk is not restricted to *P. aeruginosa* and should also occur among other *Pseudomonas* species as the corresponding *gacS*_{Δ76} mutant led to a similar phenotype in *P.fluorescens* (Zuber et al., 2003).

1 Two studies have documented the mode of interaction between the DHp domains of RetS
2 and GacS. The first study reports that RetS does not disrupt GacS homodimers, suggesting that
3 the two HKs interact as homodimers (Mancl et al., 2019). The second study reports the structure
4 of a 1:1 stoichiometric RetS_{HI}:GacS_{DHP} complex (Kaler et al., 2021). To explain this discrepancy,
5 the authors suggested that, unlike the first study, the absence of the HAMP domain destabilized
6 the GacS homodimers, resulting in the 1:1 stoichiometric RetS_{HI}:GacS_{DHP} crystal structure. The
7 HAMP domain is an essential dimerization domain in GacS (Workentine et al., 2009). Our study
8 shows compelling SEC-native MS data for the 1:1 stoichiometric GacS:RetS heterodimeric
9 complexes using GacS constructs containing the HAMP domain (Figure 6).

10 The study of Kaler et al. showed that the RetS_{HI}:GacS_{DHP} heterodimeric structure is
11 maintained by hydrophobic contacts between their DHp domains (equivalent to the homodimeric
12 interfaces). Their study also identified two critical interfacial residues on GacS DHp, I302 and
13 L309, whose substitution destabilizes the heterodimeric assembly (Kaler et al., 2021). Our study
14 shows that in addition to the DHp domain, the HAMP domain of GacS contributes a major part
15 to the interaction with RetS, as we measure a significant decrease in the RetS:GacS dissociation
16 constants in the presence of the HAMP region. The extended S-helix and HAMP domain in GacS
17 creates an apparent steric issue for the heterodimerization of the DHp domains of GacS and RetS
18 because RetS lacks a HAMP domain and its DHp domain follows on immediately after its last
19 TM helix meaning that the DHp domain of RetS will presumably be much closer to the plane of
20 the membrane than the GacS DHp domain (Figure 5). This offset in the position of the DHp
21 domains would have to be overcome by large-amplitude conformational motions in either or both
22 GacS and RetS to bring these domains together. In particular, the monomeric GacS HK might
23 undergo conformational changes that would allow multiple interfacial contacts in the formation
24 of the heterodimeric complexes; we intend to address these sophisticated dynamic changes in
25 future studies. Altogether, two binding interfaces have been found for the GacS:RetS complexes:
26 their Dhp domains heterodimerize and the GacS HAMP domain binds the HK of RetS.

27 We unveiled the essential role played by the domain ND during the autophosphorylation
28 event. Unlike ShkA, the GacS autokinase activity does not require a ligand-dependent activation,
29 suggesting that GacS_{D1} does not occupy an obstructive conformation as opposed to ShkA-Rec2.
30 The structure of RcsC HK domain containing the RcsC-ABL and PR domains, corresponds to
31 GacS ND and D1 domains (Rogov et al., 2006). In this structure, an extended linker connects the
32 two RcsC-ABL and RcsC-PR domains. The sequences of the ND domains and the linkers are
33 very poorly conserved between GacS and RcsC, but one can hypothesize that GacS unorthoHK
34 will adopt an extended linker conformation between the ND and D1 domains to promote

1
2
3
4
5
6
7
8
9
10
11
12
13
14
15
16
17
18
19
20
21
22
23
24
25
26
27
28
29
30
31
32
33
34
35
36
37
38
39
40
41
42
43
44
45
46
47
48
49
50
51
52
53
54
55
56
57
58
59
60
61
62
63
64
65

autophosphorylation and phosphotransfer. The mandatory role of GacS-ND for autophosphorylation activity suggests that GacS may differ from classical HKs. The ND domain may bind to an allosteric ligand to regulate the autokinase activity and/or interact with the inhibitory RetS hybHK. Overall, our main hypothesis is that GacS-ND propagates structural motions conferring a full GacS autokinase activity and, together with the D1 domain, may maintain the GacS cytoplasmic domains in a released conformation to favour autokinase activity.

Altogether, our findings shed light on the structural events taking place in the unorthodox membrane-associated GacS HK in its complex signal transduction pathway. These findings pave the way for a detailed characterization of an atypical trans-membrane HK that could become a major therapeutic target to prevent *PA* biofilm development.

Acknowledgments

We are grateful to Antoine Schramm, Barbara Selisko, Semeli Platsaki, Ahmad Ali Ahmad, Vincent Lombard, Véronique Zamboni, (AFMB, Marseille), Evolene Deslignière and Oscar Hernandez Alba (IPHC, Strasbourg), for fruitful discussions and technical assistance. This work was supported by the ANR projects REGALAD (ANR-14-CE09-0005) and MIDiaZONE (ANR-13-BSV8-0017), The association Vaincre la mucoviscidose - Gregory Lemarchal (RF20190502412), the CNRS, Aix-Marseille University, the University of Strasbourg, the French Infrastructures for Integrated Structural Biology (FRISBI, ANR-10-INBS-05) and for Proteomics (ProFI; ANR-10-INBS-08), and the GIS IBiSA and the Région Alsace. T.B. acknowledges the Institut de Recherches Servier for funding his PhD fellowship.

Author Contributions

F.F designed and conducted the research in structural biology, biochemistry, V.B designed and conducted the research in biochemistry, and performed structural analysis, T.B designed and performed experiments in SEC-MS. V.I.F and S.P performed in vivo studies. P.L contributed to solve GacS Xray structure, M.M.P performed binding studies by MST, Y.B. contributed to GacS structure refinement, F.V conceived the presented idea, designed the research and wrote the manuscript with support from F.F, V.B, S.L.P, S.C and Y.B.

The authors declare no competing interests

STAR methods

RESOURCE AVAILABILITY

Lead Contact

Further information and requests for resources and reagents should be directed to and will be fulfilled by the Lead Contact, Florence Vincent (fvincent.cnrs@univ-amu.fr)

Materials availability

This study did not generate new unique reagents.

Data and code availability

- X-ray diffraction data for GacS-HH1, GacS-D1, and GacS-D1 bound to BeF₃⁻ have been deposited in the PDB data bank under accession numbers 7Z8N, 7QZO and 7QZ2, respectively.
- This paper does not report original code
- Any additional information required to reanalyze the data reported in this paper is available from the lead contact upon request.

Key resources table

| REAGENT or RESOURCE | SOURCE | IDENTIFIER |
|---|------------------------|-------------------------------|
| Bacterial and virus strains | | |
| PAO1 – <i>Pseudomonas aeruginosa</i> wild type strain | (Francis et al., 2018) | PAO1 |
| <i>E. coli</i> BL21 (DE3) cells | Novagen | 69450-M |
| $\Delta retS$ derivative of PAO1 | (Francis et al., 2018) | $\Delta retS$ |
| $\Delta gacS$ derivative of PAO1 | (Francis et al., 2018) | $\Delta gacS$ |
| $\Delta retS\Delta gacS$ derivative of PAO1 | (Francis et al., 2018) | $\Delta retS\Delta gacS$ |
| <i>gacS</i> (N410D) derivative of PAO1 | (Francis et al., 2018) | <i>gacS</i> (N410D) |
| $\Delta retSgacS$ (N410D) derivative of PAO1 | (Francis et al., 2018) | $\Delta retSgacS$ (N410D) |
| <i>gacS</i> Δ 76 derivative of PAO1 | This paper | <i>gacS</i> Δ 76 |
| <i>gacS</i> Δ ND derivative of PAO1 | This paper | <i>gacS</i> Δ ND |
| $\Delta retSgacS$ Δ ND derivative of PAO1 | This paper | $\Delta retSgacS$ Δ ND |
| Biological samples | | |
| pLIC-GacSD1 | This paper | GacS _{D1} |
| pLIC-GacsS-HH1 | This paper | GacS _{HH1} |
| pLIC-GacsS-CytoFL | This paper | GacS _{cytoFL} |
| pLIC-GacsS-HH1-ND | This paper | GacS ₁₉₀₋₅₁₂ |
| pLIC-GacS190-512 | This paper | GacS _{D1} |
| pLIC-GacSD1 | This paper | GacS ₁₉₀₋₉₂₅ |
| pLIC-GacS190-925 | This paper | GacS ₁₉₀₋₉₂₅ |
| pLIC-GacS252-925 | This paper | GacS ₂₅₂₋₉₂₅ |
| pLIC-GacS280-925 | This paper | GacS ₂₈₀₋₉₂₅ |
| pLIC-RetS-H1 | This paper | RetS _{H1} |
| Chemicals, peptides, and recombinant proteins | | |

| | | |
|---|--|---|
| Isopropyl- β -D-thiogalactoside | Euromedex | EU0008-C |
| $\gamma^{32}\text{P}$ -ATP | Hartmann Analytic | FP 301 |
| ATP | Cytiva | 27205601 |
| MgCl_2 | Sigma | M8266 |
| KCl | Sigma | P3911 |
| alexa fluor 647 invitrogen | Thermofisher | A37573 |
| AMP-PNP | Merck/Roche | 10102547001 |
| kanamycin | Euromedex | EU0420 |
| LB miller | Euromedex | 0103 |
| IPTG | Euromedex | EU0008-C |
| Glycerol anhydrous | Euromedex | EU3550 |
| MES | Euromedex | EU0033 |
| MgSO_4 hexahydrate | Euromedex | P027 |
| Sodium Chloride | Euromedex | 1112-A |
| Tris base | Euromedex | 1111-C |
| Hitrap FF 5ml | Cytiva | 17531901 |
| HiLoad [®] 16/600 Superdex [®] 200 pg | Merck/Sigma-Aldrich | GE28-9893-35 |
| LAB agar No 2 Bacteriological | Neogen | MC006 |
| Nutrient broth | Oxoid | CM0001 |
| Tryptone | Sigma-Aldrich | T7293 |
| Glucose | Fisher Scientific | G/0500/53 |
| Congo Red | Thermo Scientific | 110501000 |
| Coomassie Brilliant Blue | Thermo Scientific | 20278 |
| Sucrose | Fluka | 84097 |
| Deposited data | | |
| GacS-HH1 crystal structure | This study | PBD : 7Z8N |
| GacS-D1 crystal structure | This study | PDB : 7QZO |
| GacS-D1 bound to BeF ₃ crystal structure | This study | PDB : 7QZ2 |
| Experimental models: Organisms/strains | | |
| Galleria mellonella larvae | UK Wax Worms Limited | Waxworm |
| Oligonucleotides | | |
| See Table S1 | This study | N/A |
| Recombinant DNA | | |
| pEX19Gm plasmid | (Hoang et al., 1998) | pEX19Gm |
| pLIC plasmid | (Yang et al., 2010) | RRID:Addgene_27989 |
| pRK2013 plasmid | (Figurski and Helinski, 1979) | RRID:Addgene_171139 |
| Software and algorithms | | |
| ShelXC | Schneider and Sheldrick, 2002 | https://shelx.uni-goettingen.de/ |
| ANODE | Schneider and Sheldrick, 2002; Thorn and Sheldrick, 2011 | https://shelx.uni-goettingen.de/ |
| Coot | Emsley and Cowtan, 2004 | |
| Buster | Bricogne et al, 2017 | https://www.globalphasing.com/ |
| Phaser | McCoy et al , 2007 | |
| Refmac | Murshudov et al, 1997 | |
| Molprobrity server | Chen et al., 2010 | http://molprobrity.biochem.duke.edu/ |

| | | |
|--------------------------------------|---------------------|---|
| MO Affinity software | Nanotemper | https://nanotempertech.com/monolith/ |
| Mass Lynx v4.1 | Waters | https://waters-masslynx-scen781.software.informer.com/4.1/?msclkid=317c0caba92011eca4a08e50aec48434 |
| Prism (v9) | Graphpad | www.graphpad.com |
| Other | | |
| Hitrap FF 5ml | Cytiva | 17531901 |
| HiLoad® 16/600 Superdex® 200 pg | Merck/Sigma-Aldrich | GE28-9893-35 |
| ACQUITY UPLC Protein BEH SEC Column, | Waters | 186005226 |

EXPERIMENTAL MODEL AND SUBJECT DETAILS

• Bacterial strains and growth conditions

The *E. coli* and *P. aeruginosa* bacterial strains used are listed in the key resources table. Unless stated otherwise bacteria were grown in LB broth at 37 °C. M63 (2 g/L (NH₄)₂SO₄, 13.6 g/L KH₂PO₄, 0.5 mg/L FeSO₄) supplemented with 1 mM MgSO₄, 0.5 % Casamino Acids and 0.2 % glucose was used to grow cells for the *Galleria mellonella* infection assays. Where necessary antibiotics were used at the following concentrations: gentamicin 25 µg/ml (*E. coli*) or 100 µg/ml (*P. aeruginosa*) and kanamycin 50 µg/ml (*E. coli*).

• *Galleria mellonella* model

Last instar larvae were obtained from UK Waxworms Limited and stored at 16°C until inoculation (within 1-2 days following delivery). *Galleria* for inoculation were chosen by weight (0.2 – 0.3 g) and being free from any with signs of disease (melonisation or low motility).

METHODS DETAILS

Cloning

Truncated constructs and punctual mutants of GacS and RetS used in this study, were amplified from *P. aeruginosa* PAO1 genome and cloned into pLic03 vector by Ligase Independent Cloning (LIC) which yielded to plasmids encoding for recombinant proteins fused to a 6-His tag followed by a Tobacco Etch Virus (TEV) cleavage site at their N-terminal region. Primers used for cloning and mutagenesis experiments are listed in Supplementary table S1.

Protein production

1
2
3
4
5
6
7
8
9
10
11
12
13
14
15
16
17
18
19
20
21
22
23
24
25
26
27
28
29
30
31
32
33
34
35
36
37
38
39
40
41
42
43
44
45
46
47
48
49
50
51
52
53
54
55
56
57
58
59
60
61
62
63
64
65

All constructs were expressed in *E. coli* BL21 (DE3) cells (Novagen) at 37°C. All the cells in this study, were grown in LB medium containing 50 mg.ml⁻¹ of kanamycin and induced with 200 µM IPTG at OD₆₀₀=0.6. The cells were further incubated overnight at 16°C after which cell pellets were harvested by centrifugation and disrupted by sonication. The lysate was then clarified by centrifugation and applied to a 5 ml Ni-chelating column. Proteins were eluted with 50 mM Tris pH 8, 500 mM NaCl, and 250 mM imidazole. Eluted fractions were then concentrated and further purified by size exclusion chromatography using a Superdex 16/60 S200 column equilibrated in 20mM MES pH 6.5, 500 mM NaCl and 5mM MgSO₄, for GacS constructs, 20mM Mes pH 6.5, 150 mM NaCl and 5 mM MgCl₂ for Ret_{SH1} and 20mM Mes pH 6.5, 150 mM NaCl for GacS_{D1}. Pure fractions of GacS_{HH1}, GacS_{D1} and Ret_{SH1} were analyzed by SDS-PAGE electrophoresis, pooled and concentrated to 7.4 mg/mL, 3 mg/mL, and 4.4 mg/ml using a 10 and 3 KDa cut-off centrifugation membrane (Thermoscientific). Selenomethionine-derivative GacS_{HH1} was expressed according to standard conditions for inhibiting the methionine-biosynthesis pathway and purified as for native GacS_{HH1} (Hendrickson et al., 1990).

Crystallization, data collection and processing

Crystals of GacS_{HH1} and GacS_{D1} were obtained at 4°C by vapor diffusion by screening several commercial crystallization kits, using a nanoliter sitting drops setup with automated crystallization Genesis (TECAN) and Mosquito (TTP-LabTech) robots. Drops were prepared by mixing different volumes (100, 200, and 300 nL) of protein solution with 100 nL of precipitant solutions and were equilibrated against 50 µL reservoir volume. GacS_{HH1} (7.4 mg/ml, native and SeMet derivative) was mixed with 100 nL of reservoir solution composed of 0.2 M Lithium chloride, 15–24% (w/v) PEG 3350 and 0.1 M MES pH 5.5–6.5. GacS_{D1} crystals were obtained in 0.2 M to 1.2 M Na acetate and 0.1 M HEPES from pH 7 to pH 8 in presence of 50 mM cadmium sulfate. BeF₃ bound GacS_{D1} crystals were obtained by soaking GacS_{D1} apo crystals in 5 mM BeSO₄, 30 mM NaF, 7 mM MgCl₂ and 10 mM Tris-HCl pH 9. Crystals were briefly soaked in the reservoir solution supplemented with 25% (v/v) propylene glycol for GacS_{HH1} and 25% (v/v) glycerol for GacS_{D1}, prior to flash cooling at 100K in a nitrogen gas stream. Complete data sets of selenated GacS_{HH1}, GacS_{D1}, and GacS_{D1}/BeF₃ (2.65 Å, 1.45Å, and 1.8 Å resolution, respectively) were collected on the PROXIMA 1 and 2 beamlines (SOLEIL, Saint Aubin, France). For GacS_{HH1}, two data sets of 360° were collected on the same crystal with a Chi angle offset of 18° in between the two to cover the missing cusp and improve true redundancy. For all constructs, X-ray data sets were integrated and scaled using XDS package (Kabsch, 2010), converted to MTZ format using Pointless and Aimless (Evans and Murshudov, 2013) from the CCP4 program suite

1
2
3
4
5
6
7
8
9
10
11
12
13
14
15
16
17
18
19
20
21
22
23
24
25
26
27
28
29
30
31
32
33
34
35
36
37
38
39
40
41
42
43
44
45
46
47
48
49
50
51
52
53
54
55
56
57
58
59
60
61
62
63
64
65
(Winn et al., 2011). The GacS_{HH1} unmerged intensity data were corrected for anisotropy with the STARANISO server (Tickle et al., 2018) (Table S2).

Phasing, model building and refinement

Initial Single-wavelength Anomalous Diffraction (SAD) phasing for GacS_{HH1} was calculated using the SHELXC and ANODE programs (Schneider and Sheldrick, 2002; Thorn and Sheldrick, 2011). Twenty-two selenium sites were found and the solvent-flattened electron density map at 3.3 Å resolution permitted to build an initial model using Buccaneer (Cowtan, 2006) that was improved by iterative model building using COOT (Emsley and Cowtan, 2004). Refinement rounds were performed with BUSTER including NCS restraints and TLS refinement, with three subdomains from each molecule defining a TLS group (G. Bricogne et al., 2017). The final refined model of GacS_{HH1} includes residues S221-S512 for the 4 molecules present in the asymmetric unit. High temperature factors and weak electron densities are associated with the disordered helix $\alpha 2$ N-cap (N222-E226) and the surface loops Y386-P390/G446-E450 located in the CA subdomain. GacS_{D1} structure was solved by molecular replacement with the program Phaser using the coordinates of CKL1 receiver domain (PDB ID 3MMN) as search model (rotation function Z-score: 14.4; translation function Z-score: 14.1; log likelihood gain: 3776) (McCoy et al., 2007). All structures were further refined using the REFMAC programs, and manually corrected using coot (Emsley and Cowtan, 2004; Murshudov et al., 1997). Stereochemistry of the structures was analyzed with internal modules of Coot and the Molprobit server (Chen et al., 2010). Data collection and refinement statistics are shown in Table S2.

Autokinase and kinetic assays

In vitro autophosphorylation reactions were performed in 50 mM Tris pH 8, 100 mM KCl, 5 mM MgCl₂ at room temperature. $\gamma^{32}\text{P}$ -ATP with a specific activity of 30 Ci/mmol was incubated with 10 μM of GacS_{CytoFL} and each of the truncated constructs in a 20 μL volume. The reaction was stopped after 60 mins. Separation of unincorporated ATP from the phosphorylated protein was done by SDS-PAGE. The gels were then exposed to phosphorscreens overnight and then visualized by phosphorimaging using AmershamTM TyphoonTM biomolecular Imager (GE Healthcare). A time-course assay was further performed on each construct to compare the autophosphorylation rate of GacS in presence or absence of the ND domain. Aliquots of the reactions were taken at 0, 2, 5, 10, 15, 20, 25, 30, 40, 60, 120 mins and the gel was analyzed as described previously. A competition assay was done between the cold ATP and $\gamma^{32}\text{P}$ -ATP, in

1
2
3
4
5
6
7
8
9
10
11
12
13
14
15
16
17
18
19
20
21
22
23
24
25
26
27
28
29
30
31
32
33
34
35
36
37
38
39
40
41
42
43
44
45
46
47
48
49
50
51
52
53
54
55
56
57
58
59
60
61
62
63
64
65

which 10 μM of GacS were incubated with 0.1 $\mu\text{Ci}/\mu\text{L}$ of $\gamma^{32}\text{P}$ -ATP against rising concentrations of cold ATP ranging from 0.03 to 3000 μM , for 30 mins at room temperature.

Microscale thermophoresis

Microscale Thermophoresis experiments were carried out using a Monolith NT.115 (NanoTemper technologies). GacS_{HHI} and GacS_{HHI}ND were used at a final concentration of 0.15 μM . Proteins were labeled using the Monolith NT protein labeling kit - Red NHS. AMP-PNP was titrated in 1:1 serial dilutions from 500 μM to 13 nM. For the heterodimer experiments, the GacS constructs were labelled at a final concentration of 0.15 μM . RetS_{HI} was titrated in 1:1 serial dilutions from 7 μM to 20 nM. All the experiments were performed in standard treated capillaries with 40% LED power and 80% IR-Laser power at 24°C. Laser on and off times were set at 30 secs and 5 secs respectively. All the experiments were performed in triplicate. In order to determine the dissociation constant of the interactions, MO Affinity software was used to fit the thermophoresis data for a 1:1 binding stoichiometry with the K_d model.

Size exclusion chromatography – native Mass Spectrometry experiments

Sample preparation and SEC separation.

RetS_{HI} and each of the GacS constructs were mixed in a 1:1 ratio (100 μM of each) one hour at room temperature (20°C) before injection on the SEC-MS coupling system in their native buffers. SEC was performed on an ACQUITY UPLC H-class system (Waters, Wilmslow, UK) composed of a sample manager set at 10°C, a quaternary solvent manager, a column oven set at 50°C and a TUV detector operating at 280 nm and 214 nm. The SEC system was online coupled to a Q-TOF Synapt G2 HDMS (Waters, Wilmslow, UK) mass spectrometer. SEC runs were carried out using an ACQUITY UPLC Protein BEH SEC column (2.1 x 150 mm, 1.7 μm particle size, 200 Å pore size, Waters, Wilmslow, UK) in isocratic mode with a mobile phase of 500 mM NH₄OAc (pH 7.0) at a flow rate of 0.25 ml/min over 4 mins. During MS acquisitions (from 4 to 9 mins) the flow rate was decreased to 0.10 ml/min and finally increased to 0.25 ml/min until the end of the SEC run (12 mins).

Native Mass spectrometry conditions

The Synapt G2 HDMS was used in positive mode with a capillary voltage of 3.0 kV and Z-spray source parameters were tuned in order to preserve the non-covalent interactions (40 V for the voltage cone and 6 mbar for the pressure in the interface region). MS acquisitions in native conditions were performed in the m/z range of 1000-10000 with a 1.5 scan time after an external

1 calibration using singly charged ions of a 2 g/L solution of cesium iodide in 2-propanol/water
2 (50/50 v/v). Data interpretation was performed using Mass Lynx v4.1 (Waters, Manchester, UK).
3
4

5 **Mutant generation**

6
7 Constructs containing in-frame deletions of portions of *gacS* were produced by PCR using the
8 primers described in table S1, with the deletion site flanked on either side by approximately 500bp
9 of upstream and 500bp of downstream sequence. These constructs were cloned into the allelic
10 exchange suicide plasmid, pEX19Gm. The pEX19Gm derivatives were introduced into *P.*
11 *aeruginosa* using tri-parental mating with *E. coli* containing the mobilization plasmid, pRK2013
12 (Figurski and Helinski, 1979). Sucrose and gentamycin susceptibility tests were done to isolate
13 potential *P. aeruginosa* mutants. Potential deletion mutants were checked by PCR using primers
14 outside of the initial construct used to make the deletion. These PCR products were sequenced
15 using Sanger sequencing to confirm the presence of the desired mutations. $\Delta retS$ and $\Delta gacS$
16 strains came from Francis et al., 2018 (Francis et al., 2018).
17
18
19
20
21
22
23
24
25
26

27 **Galleria mellonella infection model**

28
29 This was based on a previously described assay (Seed and Dennis, 2008). *P. aeruginosa* stains
30 were grown overnight in M63 medium supplemented with 1 mM MgSO₄, 0.5 % Casamino Acids
31 and 0.2 % glucose before being centrifuged, washed and resuspended in PBS to an OD₅₉₀=1 ±
32 0.05. This was diluted 5 x 10⁵ fold in PBS. 10 µl of the diluted bacterial suspension (20-40 CFUs)
33 were injected into the hindmost proleg of the larvae using a repeat dispenser Hamilton syringe.
34 Larvae were incubated at 37 °C and their survival was monitored. Data were analysed using
35 Kaplan-Meier survival curves. Statistical significance was assessed using the Mantel-Cox Log
36 Rank test, with Bonferroni's correction applied for multiple comparisons.
37
38
39
40
41
42
43
44
45

46 **Swarming motility assay**

47 These were performed in 140 mm diameter petri dishes containing 75 ml of media (0.5% (w/v)
48 agar (LAB Agar No.2 Bacteriological), 8g/L nutrient broth (Oxoid) and 0.5% (w/v) glucose.
49 Plates were inoculated with 0.5 ml of overnight culture grown in LB at 37 °C. Plates were
50 incubated at 30 °C for 16 hours.
51
52
53
54
55

56 **Congo Red assay**

57
58 Overnight *P. aeruginosa* cultures were diluted 100-fold and 2 ml was used to inoculate the Congo
59 red plates (140 mm diameter petri dishes containing 75 ml of 10g/L tryptone, 40 µg/mL Congo-
60
61
62
63
64
65

1 red, 20 µg/mL Coomassie brilliant blue, 1 % agar). Plates were incubated at 37 °C for 48 hours
2 and then at 20 °C for 48 hours.
3
4

5 QUANTIFICATION AND STATISTICAL ANALYSIS 6

7 Statistical details for each experiment, including replicate information, can be found in the
8 corresponding figure legend.
9

10 11 12 13 14 15 16 17 18 19 20 21 22 23 24 25 26 27 28 29 30 31 32 33 34 35 36 37 38 39 40 41 42 43 44 45 46 47 48 49 50 51 52 53 54 55 56 57 58 59 60 61 62 63 64 65 References

- 16 Ali-Ahmad, A., Fadel, F., Sebban-Kreuzer, C., Ba, M., Pélissier, G.D., Bornet, O., Guerlesquin,
17 F., Bourne, Y., Bordi, C., Vincent, F., 2017. Structural and functional insights into the
18 periplasmic detector domain of the GacS histidine kinase controlling biofilm formation in
19 *Pseudomonas aeruginosa*. *Sci. Rep.* 7, 1–13. <https://doi.org/10.1038/s41598-017-11361-3>
20
21 Anantharaman, V., Balaji, S., Aravind, L., 2006. The signaling helix: A common functional
22 theme in diverse signaling proteins. *Biol. Direct* 1, 1–16. [https://doi.org/10.1186/1745-
23 6150-1-25](https://doi.org/10.1186/1745-6150-1-25)
24
25 Armougom, F., Moretti, S., Poirot, O., Audic, S., Dumas, P., Schaeli, B., Keduas, V.,
26 Notredame, C., 2006. Expresso: automatic incorporation of structural information in
27 multiple sequence alignments using 3D-Coffee. *Nucleic Acids Res.* 34, W604-8.
28 <https://doi.org/10.1093/nar/gkl092>
29
30 Ashenberg, O., Keating, A.E., Laub, M.T., 2013. Helix Bundle Loops Determine Whether
31 Histidine Kinases Autophosphorylate in cis or in trans. *J. Mol. Biol.* 425, 1198–1209.
32 <https://doi.org/10.1016/j.jmb.2013.01.011>
33
34 Bhagirath, A.Y., Pydi, S.P., Li, Y., Lin, C., Kong, W., Chelikani, P., Duan, K., 2017.
35 Characterization of the Direct Interaction between Hybrid Sensor Kinases PA1611 and
36 RetS That Controls Biofilm Formation and the Type III Secretion System in *Pseudomonas*
37 *aeruginosa*. *ACS Infect. Dis.* 3, 162–175. <https://doi.org/10.1021/acsinfecdis.6b00153>
38
39 Bhate, M.P., Molnar, K.S., Goulian, M., DeGrado, W.F., 2015. Signal Transduction in Histidine
40 Kinases: Insights from New Structures. *Structure* 1–14.
41 <https://doi.org/10.1016/j.str.2015.04.002>
42
43 Bich, C., Baer, S., Jecklin, M.C., Zenobi, R., 2010. Probing the hydrophobic effect of
44 noncovalent complexes by mass spectrometry. *J. Am. Soc. Mass Spectrom.* 21, 286–289.
45 <https://doi.org/10.1016/j.jasms.2009.10.012>
46
47 Bilwes, A.M., Alex, L.A., Crane, B.R., Simon, M.I., 1999. Structure of CheA, a signal-

transducing histidine kinase. *Cell* 96, 131–41.

- 1
2 Bourret, R.B., 2010. Receiver domain structure and function in response regulator proteins.
3 *Curr. Opin. Microbiol.* 13, 142–149. <https://doi.org/10.1016/j.mib.2010.01.015>
4
5 Cai, Y., Hu, X., Sang, J., Chen, X., Wang, C., Shuai, J., Han, A., 2017. Conformational
6 dynamics of the essential sensor histidine kinase WalK research papers 793–803.
7 <https://doi.org/10.1107/S2059798317013043>
8
9
10 Casino, P., Miguel-romero, L., Marina, A., 2014. Visualizing autophosphorylation in histidine
11 kinases. *Nat. Commun.* 5, 1–11. <https://doi.org/10.1038/ncomms4258>
12
13 Casino, P., Rubio, V., Marina, A., 2010. The mechanism of signal transduction by two-
14 component systems. *Curr. Opin. Struct. Biol.* 20, 763–71.
15 <https://doi.org/10.1016/j.sbi.2010.09.010>
16
17
18 Chen, V.B., Arendall, W.B., Headd, J.J., Keedy, D.A., Immormino, R.M., Kapral, G.J., Murray,
19 L.W., Richardson, J.S., Richardson, D.C., 2010. MolProbity: all-atom structure validation
20 for macromolecular crystallography. *Acta Crystallogr. D. Biol. Crystallogr.* 66, 12–21.
21 <https://doi.org/10.1107/S0907444909042073>
22
23
24 Cowtan, K., 2006. The Buccaneer software for automated model building. 1. Tracing protein
25 chains. *Acta Crystallogr. D. Biol. Crystallogr.* 62, 1002–11.
26 <https://doi.org/10.1107/S0907444906022116>
27
28
29 Dubey, B.N., Agustoni, E., Böhm, R., Kaczmarczyk, A., Mangia, F., von Arx, C., Jenal, U.,
30 Hiller, S., Plaza-Menacho, I., Schirmer, T., 2019. Hybrid histidine kinase activation by
31 cyclic di-GMP-mediated domain liberation. *Proc. Natl. Acad. Sci.* 201911427.
32 <https://doi.org/10.1073/pnas.1911427117>
33
34
35 Dutta, R., Inouye, M., 1996. Reverse Phosphotransfer from OmpR to EnvZ in a
36 Kinase-/Phosphatase+ Mutant of EnvZ (EnvZ•N347D), a Bifunctional Signal Transducer
37 of *Escherichia coli*. *J. Biol. Chem.* 271, 1424–1429. <https://doi.org/10.1074/jbc.271.3.1424>
38
39
40 Emsley, P., Cowtan, K., 2004. Coot: model-building tools for molecular graphics. *Acta*
41 *Crystallogr D Biol Crystallogr* 60, 2126–2132.
42 <https://doi.org/10.1107/S0907444904019158>
43
44
45 Evans, P.R., Murshudov, G.N., 2013. How good are my data and what is the resolution? *Acta*
46 *Crystallogr. D. Biol. Crystallogr.* 69, 1204–14.
47 <https://doi.org/10.1107/S0907444913000061>
48
49
50 Figurski, D.H., Helinski, D.R., 1979. Replication of an origin-containing derivative of plasmid
51 RK2 dependent on a plasmid function provided in trans. *Proc. Natl. Acad. Sci.* 76, 1648–
52 1652. <https://doi.org/10.1073/pnas.76.4.1648>
53
54
55
56
57
58
59
60
61
62
63
64
65

- Francis, V.I., Waters, E.M., Finton-James, S.E., Gori, A., Kadioglu, A., Brown, A.R., Porter, S.L., 2018. Multiple communication mechanisms between sensor kinases are crucial for virulence in *Pseudomonas aeruginosa*. *Nat. Commun.* 9, 2219.
<https://doi.org/10.1038/s41467-018-04640-8>
- G. Bricogne, Blanc, E., Brandl, M., Flensburg, C., Keller, P., Paciorek, W., Roversi, P., Sharff, A., Smart, O.S., Vonrhein, C., T.O. Womack, 2017. BUSTER. Global Phasing Ltd, Cambridge, United Kingdom, p. version 2.10.3.
- Gao, R., Stock, A.M., 2010. Molecular strategies for phosphorylation-mediated regulation of response regulator activity. *Curr. Opin. Microbiol.* 13, 160–167.
<https://doi.org/10.1016/j.mib.2009.12.009>
- Gooderham, W.J., Hancock, R.E.W., 2009. Regulation of virulence and antibiotic resistance by two-component regulatory systems in *Pseudomonas aeruginosa*. *FEMS Microbiol Rev* 33, 279–294.
- Goodman, A.L., Merighi, M., Hyodo, M., Ventre, I., Filloux, A., Lory, S., 2009. Direct interaction between sensor kinase proteins mediates acute and chronic disease phenotypes in a bacterial pathogen. *Genes Dev* 23, 249–259. <https://doi.org/10.1101/gad.1739009>
- Gushchin, I., Melnikov, I., Polovinkin, V., Ishchenko, A., Yuzhakova, A., Buslaev, P., Bourenkov, G., Grudinin, S., Round, E., Balandin, T., Borshchevskiy, V., Willbold, D., Leonard, G., Büldt, G., Popov, A., Gordeliy, V., 2017a. Mechanism of transmembrane signaling by sensor histidine kinases. *Science* (80-.). 356, eaah6345.
<https://doi.org/10.1126/science.aah6345>
- Heeb, S., Haas, D., 2001. Regulatory Roles of the GacS/GacA Two-Component System in Plant-Associated and Other Gram-Negative Bacteria. *Mol. Plant-Microbe Interact.* 14, 1351–1363. <https://doi.org/10.1094/MPMI.2001.14.12.1351>
- Hendrickson, W.A., Horton, J.R., LeMaster, D.M., 1990. Selenomethionyl proteins produced for analysis by multiwavelength anomalous diffraction (MAD): a vehicle for direct determination of three-dimensional structure. *EMBO J.* 9, 1665–72.
- Hoang, T.T., Karkhoff-Schweizer, R.R., Kutchma, A.J., Schweizer, H.P., 1998. A broad-host-range Flp-FRT recombination system for site-specific excision of chromosomally-located DNA sequences: application for isolation of unmarked *Pseudomonas aeruginosa* mutants. *Gene* 212, 77–86. [https://doi.org/10.1016/S0378-1119\(98\)00130-9](https://doi.org/10.1016/S0378-1119(98)00130-9)
- Jacob-Dubuisson, F., Mechaly, A., Betton, J.-M., Antoine, R., 2018. Structural insights into the signalling mechanisms of two-component systems. *Nat. Rev. Microbiol.* 16, 585–593.
<https://doi.org/10.1038/s41579-018-0055-7>

- 1
2
3
4
5
6
7
8
9
10
11
12
13
14
15
16
17
18
19
20
21
22
23
24
25
26
27
28
29
30
31
32
33
34
35
36
37
38
39
40
41
42
43
44
45
46
47
48
49
50
51
52
53
54
55
56
57
58
59
60
61
62
63
64
65
- Kabsch, W., 2010. XDS. *Acta Crystallogr. Sect. D Biol. Crystallogr.* 66, 125–132.
<https://doi.org/10.1107/S0907444909047337>
- Kim, D.J., Forst, S., 2001. Genomic analysis of the histidine kinase family in bacteria and archaea. *Microbiology* 147, 1197–1212. <https://doi.org/10.1099/00221287-147-5-1197>
- Kitten, T., Kinscherf, T.G., McEvoy, J.L., Willis, D.K., 1998. A newly identified regulator is required for virulence and toxin production in *Pseudomonas syringae*. *Mol Microbiol* 28, 917–929.
- Lapouge, K., Schubert, M., Allain, F.H.-T.-. T., Haas, D., 2008. Gac/Rsm signal transduction pathway of gamma-proteobacteria: from RNA recognition to regulation of social behaviour. *Mol Microbiol* 67, 241–253.
- Mancl, J.M., Ray, W.K., Helm, R.F., Schubot, F.D., 2019. Helix Cracking Regulates the Critical Interaction between RetS and GacS in *Pseudomonas aeruginosa*. *Structure* 1–9.
<https://doi.org/10.1016/j.str.2019.02.006>
- Marina, A., Waldburger, C.D., Hendrickson, W.A., 2005. Structure of the entire cytoplasmic portion of a sensor histidine-kinase protein. *EMBO J.* 24, 4247–59.
<https://doi.org/10.1038/sj.emboj.7600886>
- Marty, M.T., Baldwin, A.J., Marklund, E.G., Hochberg, G.K.A., Benesch, J.L.P., Robinson, C. V., 2015. Bayesian Deconvolution of Mass and Ion Mobility Spectra: From Binary Interactions to Polydisperse Ensembles. *Anal. Chem.* 87, 4370–4376.
<https://doi.org/10.1021/acs.analchem.5b00140>
- McCoy, A.J., Grosse-Kunstleve, R.W., Adams, P.D., Winn, M.D., Storoni, L.C., Read, R.J., 2007. Phaser crystallographic software. *J. Appl. Crystallogr.* 40, 658–674.
<https://doi.org/10.1107/S0021889807021206>
- McLachlan, A.D., Stewart, M., 1975. Tropomyosin coiled-coil interactions: evidence for an unstaggered structure. *J. Mol. Biol.* 98, 293–304.
- Micek, S.T., Wunderink, R.G., Kollef, M.H., Chen, C., Rello, J., Chastre, J., Antonelli, M., Welte, T., Clair, B., Ostermann, H., Calbo, E., Torres, A., Menichetti, F., Schramm, G.E., Menon, V., 2015. An international multicenter retrospective study of *Pseudomonas aeruginosa* nosocomial pneumonia: impact of multidrug resistance. *Crit. Care* 19, 219.
<https://doi.org/10.1186/s13054-015-0926-5>
- Murshudov, G.N., Vagin, A.A., Dodson, E.J., 1997. Refinement of macromolecular structures by the maximum-likelihood method. *Acta Crystallogr D Biol Crystallogr* 53, 240–255.
<https://doi.org/10.1107/S0907444996012255>
- Nathwani, D., Raman, G., Sulham, K., Gavaghan, M., Menon, V., 2014. Clinical and economic

- 1 consequences of hospital-acquired resistant and multidrug-resistant *Pseudomonas*
2 *aeruginosa* infections: a systematic review and meta-analysis. *Antimicrob. Resist. Infect.*
3 *Control* 3, 32. <https://doi.org/10.1186/2047-2994-3-32>
- 4
5 Nguyen, M.-P., Yoon, J.-M., Cho, M.-H., Lee, S.-W., 2015. Prokaryotic 2-component systems
6 and the OmpR/PhoB superfamily. *Can. J. Microbiol.* 61, 799–810.
7
8 <https://doi.org/10.1139/cjm-2015-0345>
- 9
10 Podgornaia, A.I., Casino, P., Marina, A., Laub, M.T., 2013. Structural basis of a rationally
11 rewired protein-protein interface critical to bacterial signaling. *Structure* 21, 1636–1647.
- 12
13 Rogov, V. V., Rogova, N.Y., Bernhard, F., Koglin, A., Löhr, F., Dötsch, V., 2006. A New
14 Structural Domain in the *Escherichia coli* RcsC Hybrid Sensor Kinase Connects Histidine
15 Kinase and Phosphoreceiver Domains. *J. Mol. Biol.* 364, 68–79.
16
17 <https://doi.org/10.1016/j.jmb.2006.07.052>
- 18
19 Ryan Kaler, K.M., Nix, J.C., Schubot, F.D., 2021. RetS inhibits *Pseudomonas aeruginosa*
20 biofilm formation by disrupting the canonical histidine kinase dimerization interface of
21 GacS. *J. Biol. Chem.* 101193. <https://doi.org/10.1016/j.jbc.2021.101193>
- 22
23 Saita, E., Abriata, L.A., Tsai, Y.T., Trajtenberg, F., Lemmin, T., Buschiazzo, A., Dal Peraro,
24 M., de Mendoza, D., Albanesi, D., 2015. A coiled coil switch mediates cold sensing by the
25 thermosensory protein DesK. *Mol. Microbiol.* 98, 258–271.
26
27 <https://doi.org/10.1111/mmi.13118>
- 28
29 Schneider, T.R., Sheldrick, G.M., 2002. Substructure solution with SHELXD. *Acta Crystallogr.*
30 *Sect. D-Biological Crystallogr.* 58, 1772–1779.
- 31
32 Seed, K.D., Dennis, J.J., 2008. Development of *Galleria mellonella* as an alternative infection
33 model for the *Burkholderia cepacia* complex. *Infect. Immun.* 76, 1267–75.
34
35 <https://doi.org/10.1128/IAI.01249-07>
- 36
37 Sousa, A., Pereira, M., 2014. *Pseudomonas aeruginosa* Diversification during Infection
38 Development in Cystic Fibrosis Lungs—A Review. *Pathogens* 3, 680–703.
39
40 <https://doi.org/10.3390/pathogens3030680>
- 41
42 Southall, N.T., Dill, K.A., Haymet, A.D.J., 2002. A View of the Hydrophobic Effect. *J. Phys.*
43 *Chem. B* 106, 521–533. <https://doi.org/10.1021/jp015514e>
- 44
45 Stewart, V., Chen, L.-L., 2010. The S Helix Mediates Signal Transmission as a HAMP Domain
46 Coiled-Coil Extension in the NarX Nitrate Sensor from *Escherichia coli* K-12. *J. Bacteriol.*
47 192, 734–745. <https://doi.org/10.1128/JB.00172-09>
- 48
49 Stock, A.M., Robinson, V.L., Goudreau, P.N., 2000. Two-component signal transduction. *Annu*
50 *Rev Biochem* 69, 183–215.
- 51
52
53
54
55
56
57
58
59
60
61
62
63
64
65

- 1 Thomas, F., Niitsu, A., Oregioni, A., Bartlett, G.J., Woolfson, D.N., 2017. Conformational
2 Dynamics of Asparagine at Coiled-Coil Interfaces. *Biochemistry* 56, 6544–6554.
3 <https://doi.org/10.1021/acs.biochem.7b00848>
4
- 5 Thorn, A., Sheldrick, G.M., 2011. ANODE: anomalous and heavy-atom density calculation. *J.*
6 *Appl. Crystallogr.* 44, 1285–1287. <https://doi.org/10.1107/S0021889811041768>
7
- 8 Tickle, I.J., Flensburg, C., Keller, P., Paciorek, W., Sharff, A., Vonrhein, C., Bricogne, G.,
9 2018. STARANISO.
10
- 11 Ventre, I., Goodman, A.L., Vallet-Gely, I., Vasseur, P., Soscia, C., Molin, S., Bleves, S.,
12 Lazdunski, A., Lory, S., Filloux, A., 2006. Multiple sensors control reciprocal expression
13 of *Pseudomonas aeruginosa* regulatory RNA and virulence genes. *Proc Natl Acad Sci U S*
14 *A* 103, 171–176. <https://doi.org/10.1073/pnas.0507407103>
15
- 16 Wang, C., Sang, J., Wang, J., Su, M., Downey, J.S., Wu, Q., Wang, S., Cai, Y., Xu, X., Wu, J.,
17 Senadheera, D.B., Cvitkovitch, D.G., Chen, L., Goodman, S.D., Han, A., 2013.
18 Mechanistic Insights Revealed by the Crystal Structure of a Histidine Kinase with Signal
19 Transducer and Sensor Domains 11. <https://doi.org/10.1371/journal.pbio.1001493>
20
- 21 Winn, M.D., Ballard, C.C., Cowtan, K.D., Dodson, E.J., Emsley, P., Evans, P.R., Keegan, R.M.,
22 Krissinel, E.B., Leslie, A.G.W., McCoy, A., McNicholas, S.J., Murshudov, G.N., Pannu,
23 N.S., Potterton, E.A., Powell, H.R., Read, R.J., Vagin, A., Wilson, K.S., 2011. Overview of
24 the CCP4 suite and current developments. *Acta Crystallogr. D. Biol. Crystallogr.* 67, 235–
25 42. <https://doi.org/10.1107/S0907444910045749>
26
- 27 Winstanley, C., O'Brien, S., Brockhurst, M.A., 2016. *Pseudomonas aeruginosa* Evolutionary
28 Adaptation and Diversification in Cystic Fibrosis Chronic Lung Infections. *Trends*
29 *Microbiol.* 24, 327–337. <https://doi.org/10.1016/j.tim.2016.01.008>
30
- 31 Workentine, M.L., Chang, L., Ceri, H., Turner, R.J., 2009. The GacS-GacA two-component
32 regulatory system of *Pseudomonas fluorescens*: a bacterial two-hybrid analysis. *FEMS*
33 *Microbiol Lett* 292, 50–56. <https://doi.org/10.1111/j.1574-6968.2008.01445.x>
34
- 35 Yang, J., Zhang, Z., Zhang, X.A., Luo, Q., 2010. A ligation-independent cloning method using
36 nicking DNA endonuclease. *Biotechniques* 49, 817–821.
37 <https://doi.org/10.2144/000113520>
38
- 39 Zhou, Q., Ames, P., Parkinson, J.S., 2009. Mutational analyses of HAMP helices suggest a
40 dynamic bundle model of input-output signalling in chemoreceptors. *Mol. Microbiol.* 73,
41 801–814. <https://doi.org/10.1111/j.1365-2958.2009.06819.x>
42
- 43 Zschiedrich, C.P., Keidel, V., Szurmant, H., 2016. Molecular Mechanisms of Two-Component
44 Signal Transduction. *J. Mol. Biol.* 428, 3752–3775.
45
46
47
48
49
50
51
52
53
54
55
56
57
58
59
60
61
62
63
64
65

1 Zuber, S., Carruthers, F., Keel, C., Mattart, A., Blumer, C., Pessi, G., Gigot-Bonnefoy, C.,
2
3 Schnider-Keel, U., Heeb, S., Reimann, C., Haas, D., 2003. GacS sensor domains
4 pertinent to the regulation of exoproduct formation and to the biocontrol potential of
5
6 *Pseudomonas fluorescens* CHA0. *Mol Plant Microbe Interact* 16, 634–644.
7
8
9

10
11 **Figures legends**
12

13
14 **Figure 1. GacS and RetS HK modularity, Overall structure of GacS_{HH1} and GacS_{D1}.** A-
15 Schematic representation of GacS unorthoHK and RetS hybHK showing the different domains of
16 GacS and RetS drawn to scale, with the phosphorylatable residues histidines (H) and aspartate (D)
17 shown in green on GacS. B- Overall view of the elongated GacS dimeric assembly with each subunit
18 colored in yellow and green showing, from the N- to C-terminus, the HAMP, S-helix, DHp and CA
19 domains. The phosphorylatable histidine is show with spheres. C- Superimposition of GacS_{D1} apo
20 with GacS_{D1} bound to BeF₃⁻. In green GacS_{D1} bound to BeF₃⁻, the residues involved in BeF₃⁻ binding
21 are shown in sticks. In grey GacS_{D1} apo, the original position of the binding residues is shown in
22 sticks and the motion made by H750 upon BeF₃⁻ binding is shown with a red arrow.
23
24
25
26
27
28
29
30

31
32 **Figure 2. Structure-based assignment of GacS_{HH1} coiled-coil heptads.** A- Register showing the
33 GacS_{HH1} coiled-coil heptad repeats along the HAMP and S-Helix sequences colored in magenta and
34 yellow, and the overlapping region between the HAMP domain $\alpha 2$ and the S-helix in light brown.
35 Hydrophilic residues at position d of the S-helix domain are highlighted in red. B- View of the
36 HAMP $\alpha 2$, S-helix and DHp $\alpha 3/\alpha 4$ dimer. C- Close-up view of the S-helix residues (blue) buried at
37 the dimeric interface dominated by hydrophobic interactions. The two pairs of hydrophilic residues
38 are labelled in red. The experimental anomalous electron density maps contoured at 4 σ (cyan) is
39 displayed near the two SeMet residues. D- Sequence alignment of the GacS HAMP/S-helix regions
40 with the homologous BarA, NarQ and NarX HKs showing the conservation score above the
41 sequences. Red indicates highly conserved and blue weakly conserved residues. The boundaries of
42 each domain and the residues in position a and d are indicated. The position of the stutter denoted
43 a/d at residue L238 in GacS_{HH1} and the QAT signature motif in the conserved core of the S-helix
44 are highlighted in red.
45
46
47
48
49
50
51
52
53
54
55

56
57
58 **Figure 3: Phenotypic analysis of *gacS* mutants.** A-D Representative images of the swarming of
59 the wild-type PAO1 strain and its mutant derivatives. E-G Representative images of congo red
60
61
62
63
64
65

1 agar plates of the wild type PAO1 strain and its mutant derivatives. Experiments were repeated
2 three times.
3
4

5 **Figure 4. Relative survival rate of *P. aeruginosa*-infected *G. mellonella* larvae.** Relative survival
6 rates are depicted as Kaplan-Meier curves of the different groups with PAO1 (cyan), $\Delta gacS$ (pink),
7 $\Delta retS$ (green), the $gacS_{\Delta 76}$ variant (grey) and PBS control (black). Experiments were done in
8 replicates and relative survival was plotted against the incubation time.
9
10
11
12

13 **Figure 5: 3D structures from GacS and RetS HKs and full-length models.** A- The solved
14 structural domains of GacS are shown in cartoon embedded in a surface, the unsolved domains
15 structures are represented in light blue squares. B- Crystals structures of RetS HK, the unsolved
16 receiver domains D1 and D2 are represented in light blue squares. The shift of 90Å between
17 GacSH1 and RetSH1 is represented by an arrow.
18
19
20
21
22
23

24 **Figure 6. Online SEC-native MS analysis of the different oligomeric species.** SEC
25 chromatograms of A- GacS_{CytoFL}/RetS_{HI}, B- GacS_{HH1}/RetS_{HI} and C- GacS₂₅₂₋₉₂₅/RetS_{HI} samples.
26 The constructs used for the experiments and their homodimeric or heterodimeric states are depicted
27 with colored domains as described in figure 1. Native mass spectra of the second SEC peak
28 corresponding to the presence/absence of a GacS:RetS complex for D- GacS_{CytoFL}, E- GacS_{HH1} and
29 F- GacS₂₅₂₋₉₂₅. G- The experimental and theoretical molecular masses of homodimeric and complex
30 species are summarized. Native mass spectra of homodimeric species are provided in Fig. S2. Due
31 to the high heterogeneity of the GacS₂₅₂₋₉₂₅ construct many different masses were calculated for the
32 GacS₂₅₂₋₉₂₅:GacS₂₅₂₋₉₂₅ and GacS₂₅₂₋₉₂₅:RetS_{HI} complexes. Mass spectra of GacS constructs are
33 provided in figure S2 and related complex deconvolutions in figure S7.
34
35
36
37
38
39
40
41
42
43
44

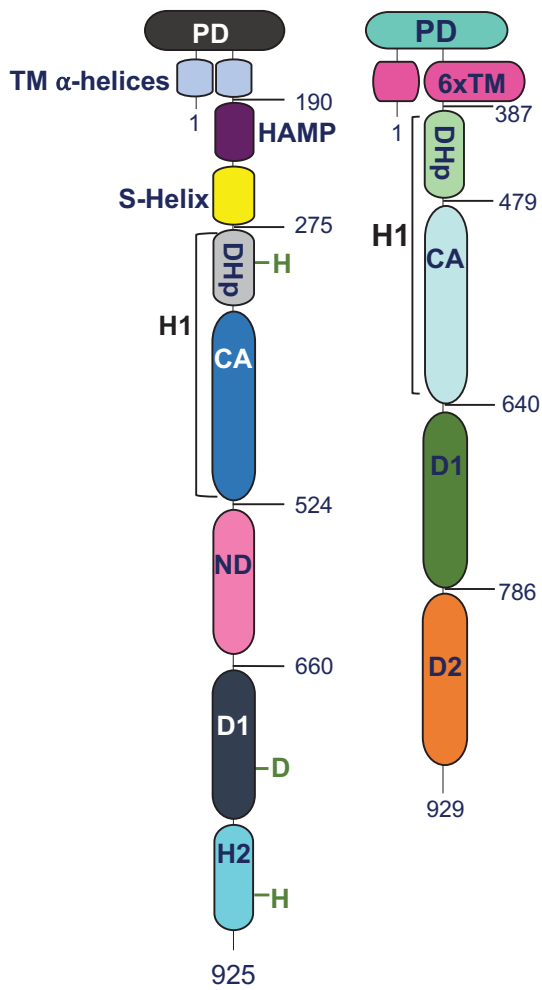
45 **Figure 7. Dose-response curves for binding interactions determined by microscale**
46 **thermophoresis.** A- Binding of RetS_{HI} to the labeled GacS constructs. All the curves are shown as
47 the fraction bound against the ligand's concentration. B- Binding of AMP-PNP to the fluorescently
48 labeled GacS_{HH1} and GacS_{HH1ND} constructs. Curves are derived from the specific change in the
49 thermophoretic mobility upon titration of AMP-PNP. For each measurement, 3 replicates are
50 displayed as average values and error bars representing the standard deviation.
51
52
53
54
55
56
57

58 **Figure 8. Radioactive-based assays.** A- Time-course autophosphorylation kinetics of the four
59 GacS constructs, as measured by autoradiography using $\gamma^{32}\text{P}$ -ATP, B- GacS_{Chimera}, GacS_{CytoFLAND}
60
61
62
63
64
65

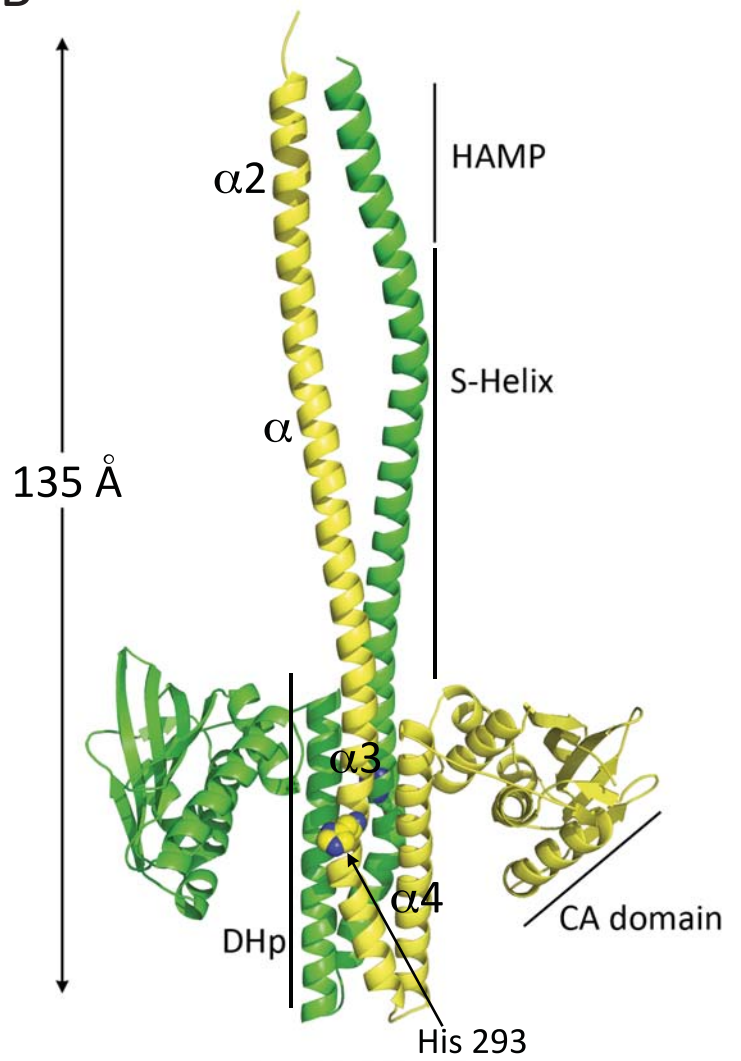
1 autophosphorylation profiles after 60 min incubation. C- Competition-based assay between $\gamma^{32}\text{P}$ -
2 ATP at 0.1 $\mu\text{Ci}/\mu\text{L}$ against cold ATP from 0.03 μM to 3000 μM after 30 min incubation using the
3 GacS_{HHIND} variant. Experiments were done in replicates. SDS-PAGE gels are shown below to
4 indicate equal protein loading.
5
6
7
8
9
10
11
12
13
14
15
16
17
18
19
20
21
22
23
24
25
26
27
28
29
30
31
32
33
34
35
36
37
38
39
40
41
42
43
44
45
46
47
48
49
50
51
52
53
54
55
56
57
58
59
60
61
62
63
64
65

Figure 1

A-



B-



C-

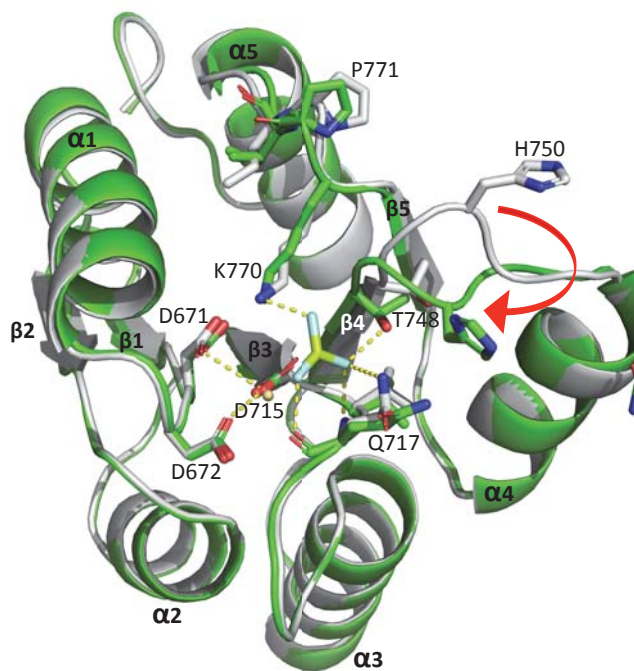
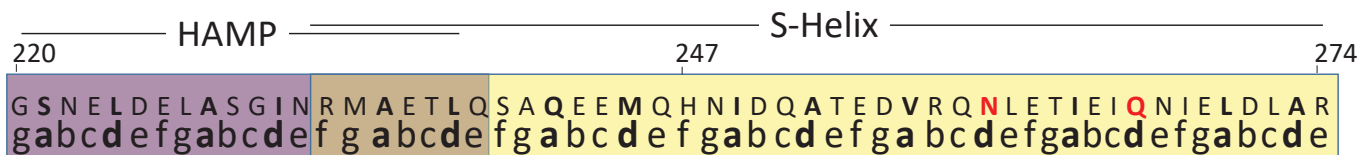
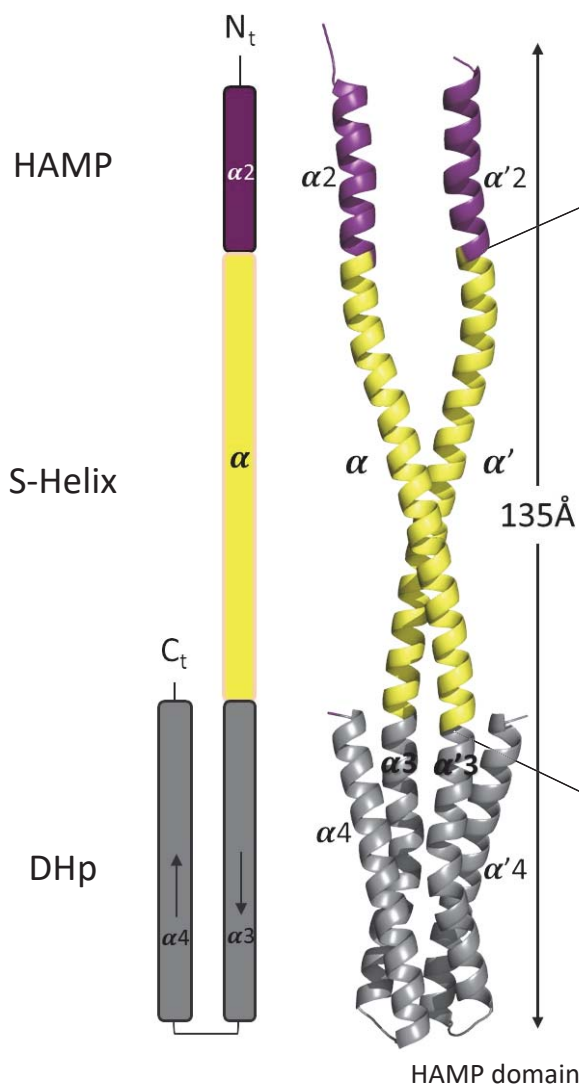


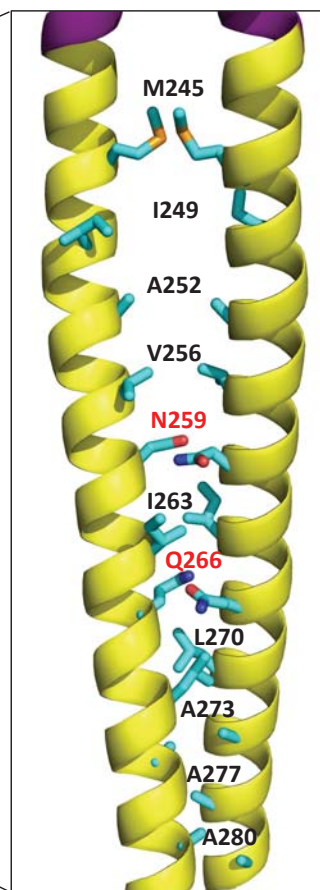
Figure 2
A-



B-



C-



D-

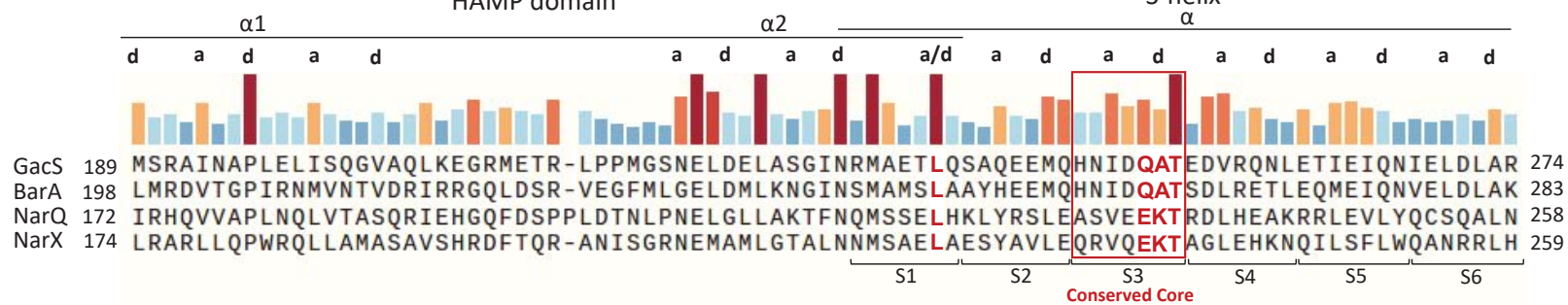
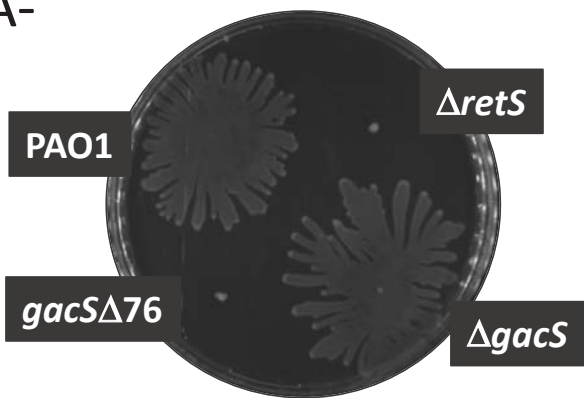
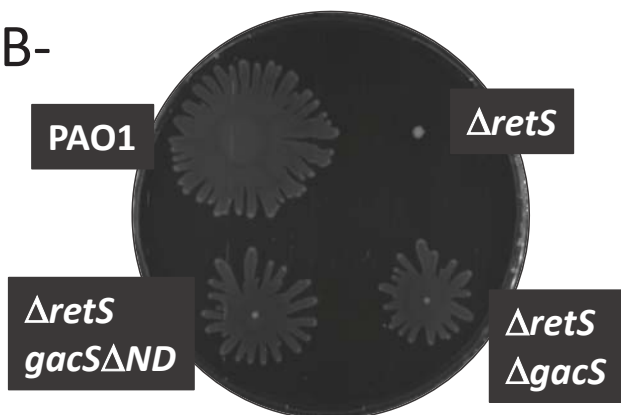


Figure 3

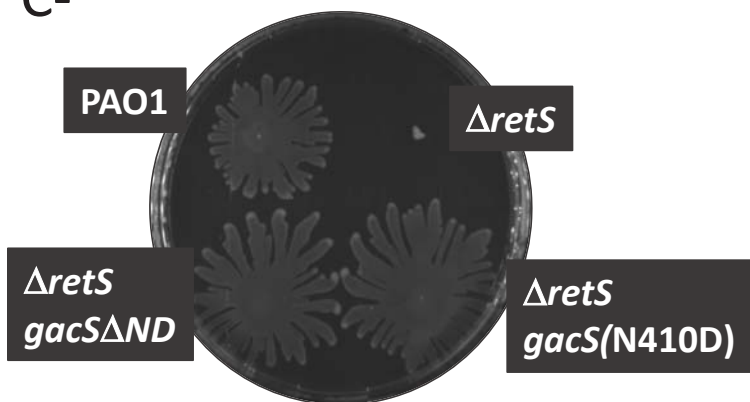
A-



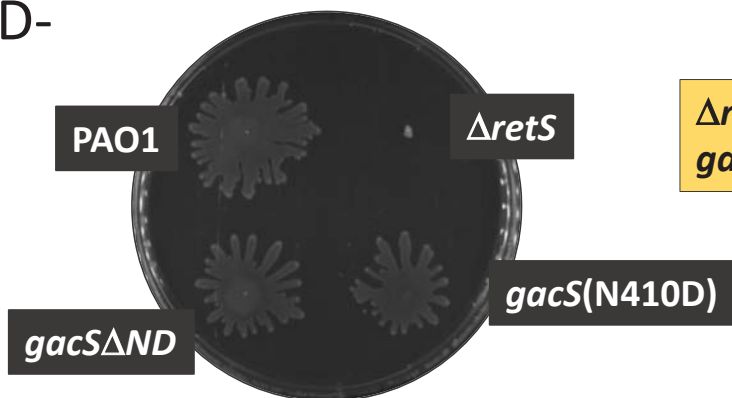
B-



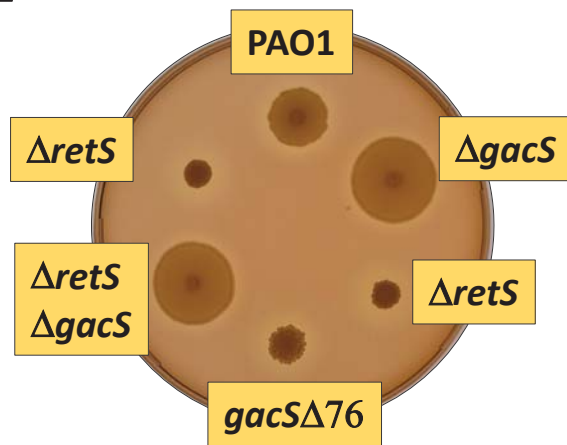
C-



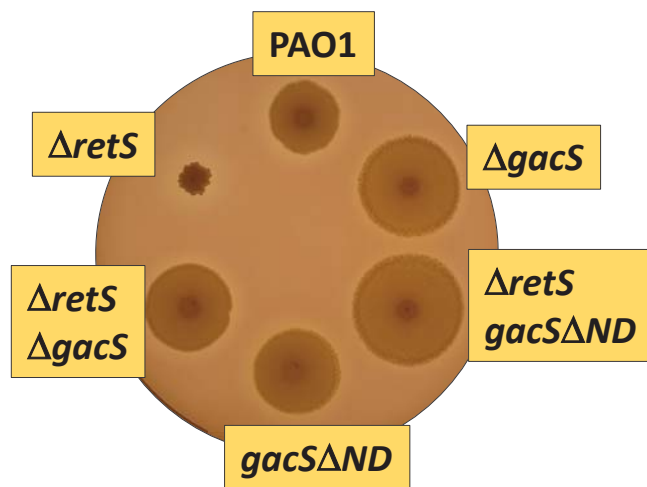
D-



E-



F-



G-

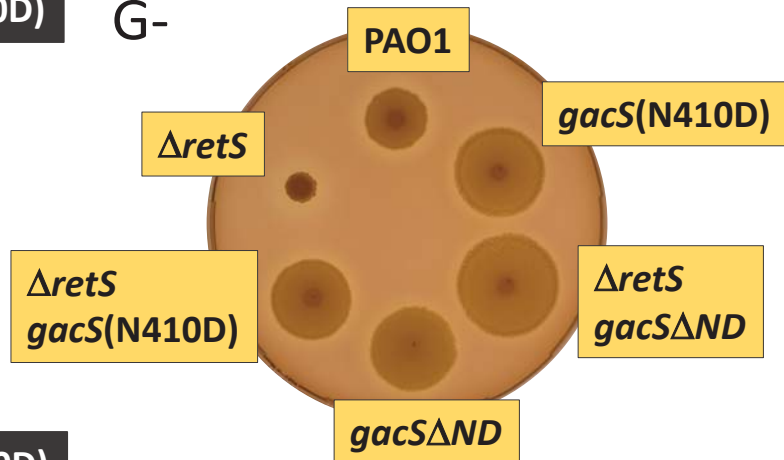


Figure 4

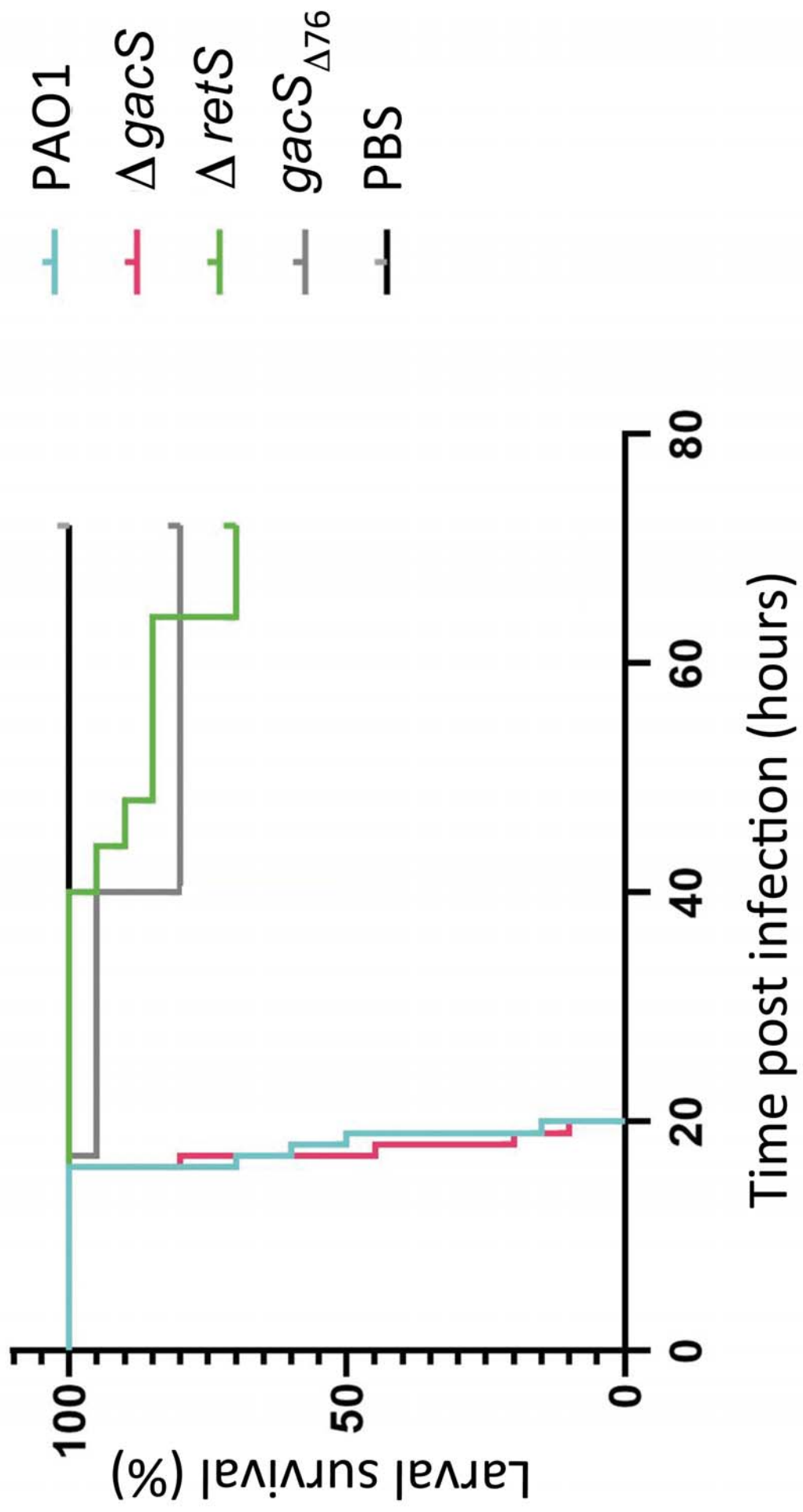
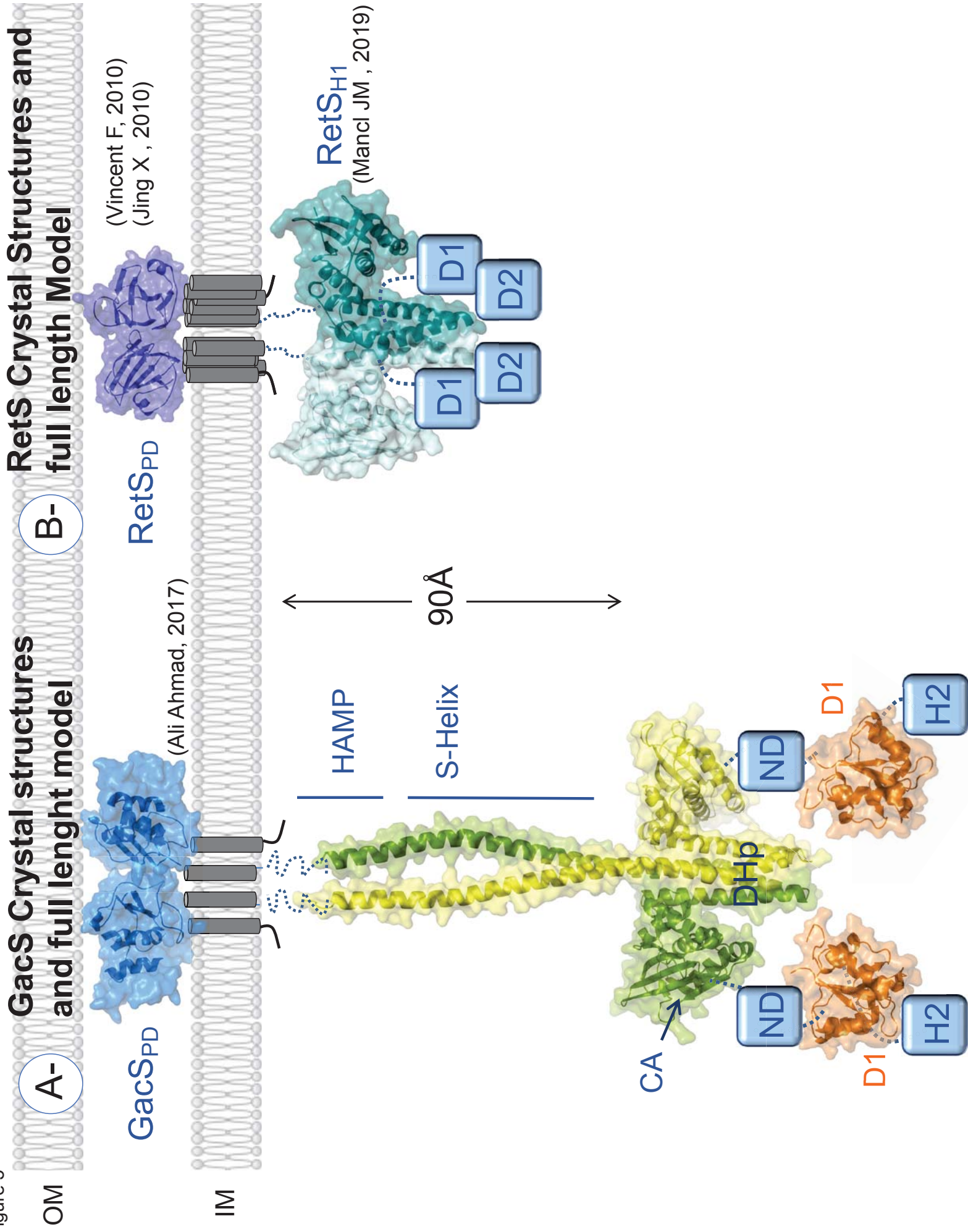
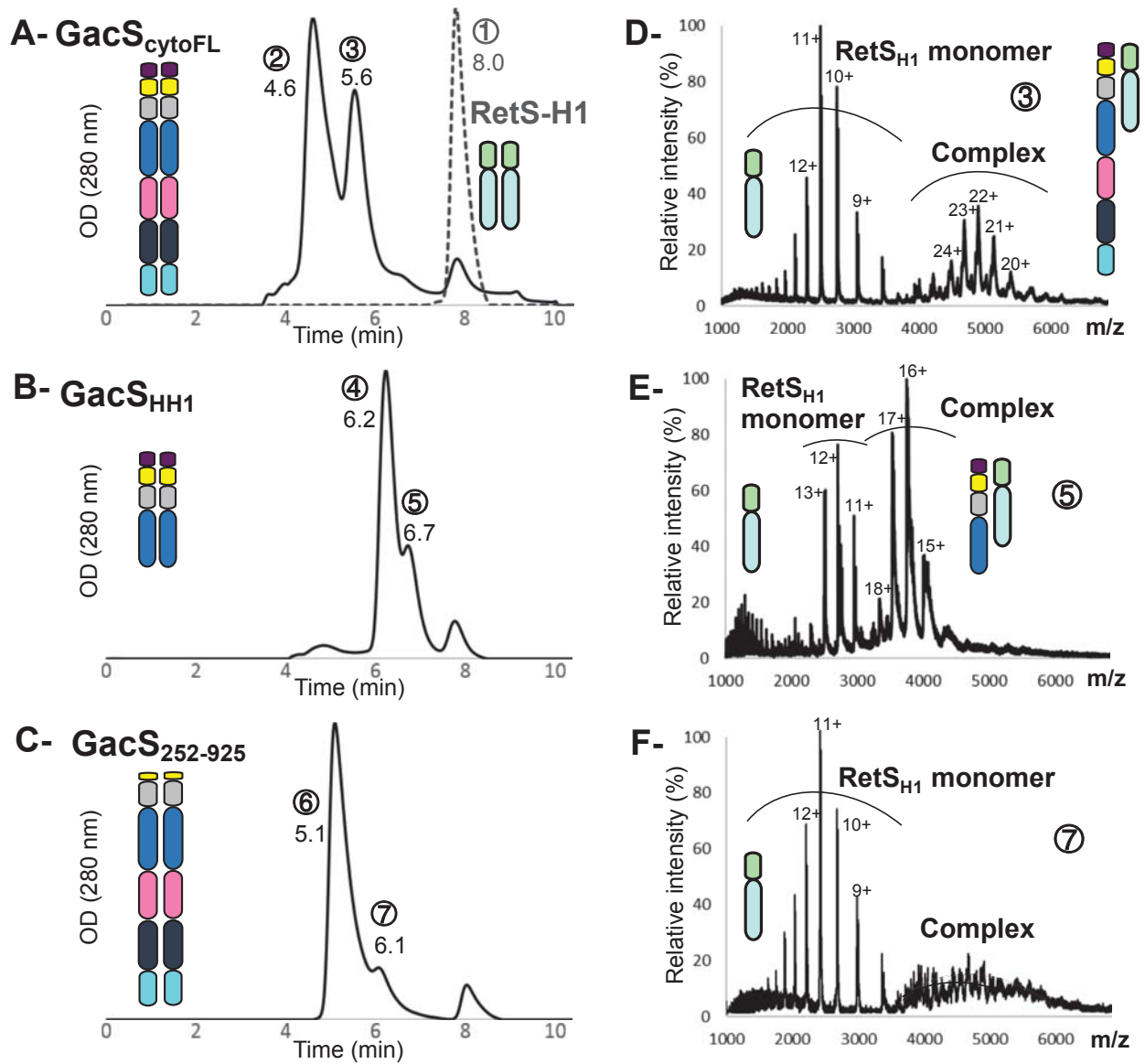


Figure 5





G-

| Species | Peak/ Time (min) | Measured mass (Da) | Theoretical mass(Da) |
|---|------------------|--------------------|---|
| Homodimer RetS_{H1} | ① 8.0 | 55,030.1 ±0.7 | 55,030.6 |
| Homodimer GacS_{cytoFL} | ② 4.6 | 160,189.0 ±11.3 | 159,824.4 (160,180.4 +2 gluconoylations) |
| Homodimer GacS_{HH1} | ④ 6.2 | 64,914.1 ±0.6 | 64,913.2 |
| Complex RetS_{H1}+ GacS_{cytoFL} | ③ 5.6 | 107,614.4 ±3.5 | 107,425.5 (107,605.5 +1 gluconoylation) |
| Complex RetS_{H1}+ GacS_{HH1} | ⑤ 6.7 | 59,973.2 ±1.6 | 59,971.9 |
| Homodimer GacS₂₅₂₋₉₂₅ | ⑥ 5.1 | ≈150,000* | 147,521 |
| Complex RetS_{H1}+ GacS₂₅₂₋₉₂₅ | ⑦ 6.1 | ≈103,000* | 101,276 |

Figure 7

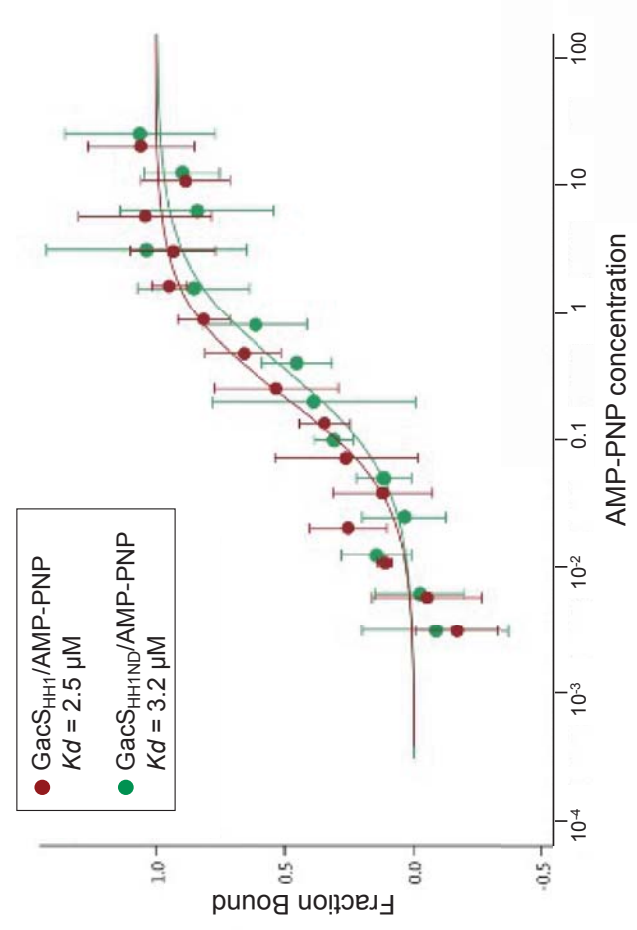
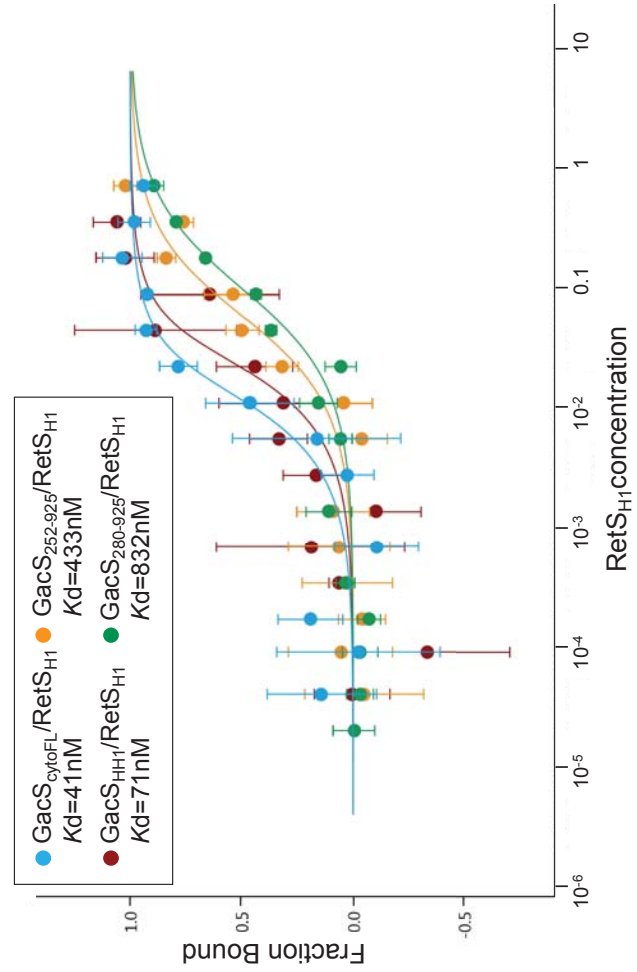
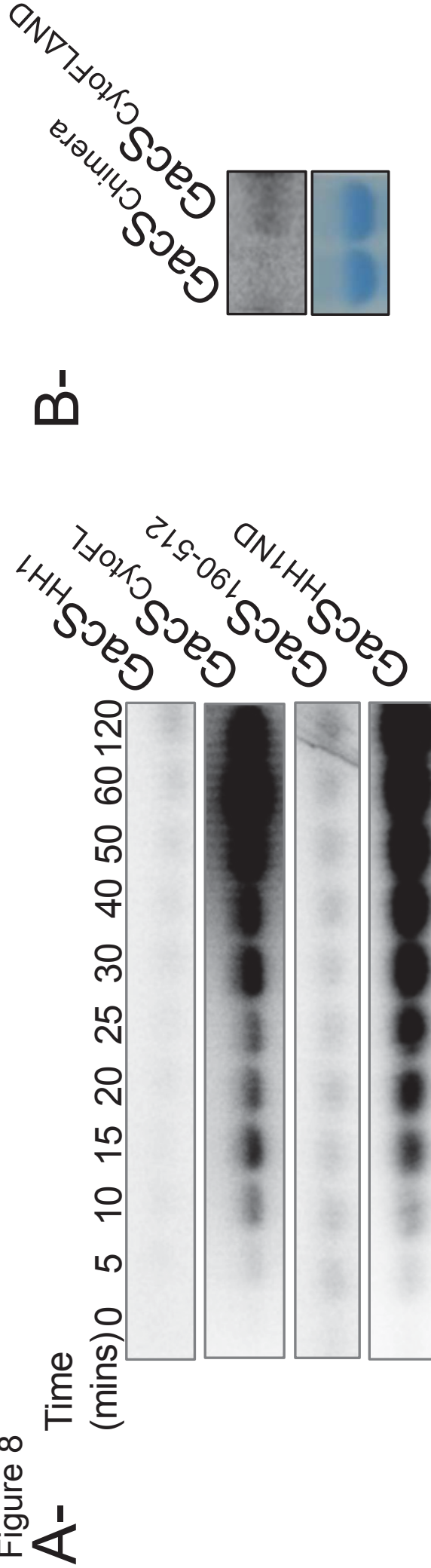
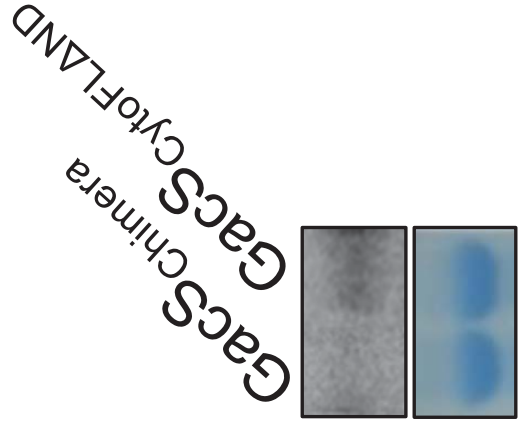


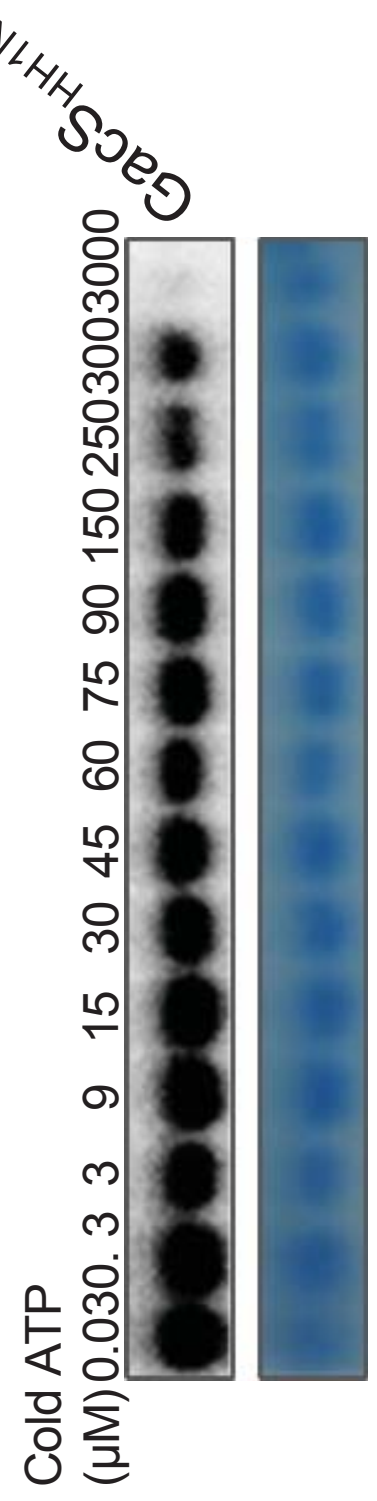
Figure 8



B-



C-



Supplementary tables**Table S1. Primers used in this study, related to the STAR Methods section.**

| Constructs | Residues | Forward primer |
|-------------------------|----------|--|
| | | Reverse primer |
| GacS ₁₉₀₋₅₁₂ | 190-512 | 5'-TACTTCCAATCAATGAGCCGCGCGATCAACGCGCCG-3' 5'-CGTGGCACCAGAGCGTTATTAACCTTTTCGGCAGACTCAG-3' |
| GacS _{CytoFL} | 220-925 | 5'-TACTTCCAATCAATGGGCAGCAACGAGCTG-3' 5'-TATCCACCTTTACTGTTATTATCAGAGTTCGCTGGAGTC-3' |
| GacS _{HH1} | 220-512 | 5'-TACTTCCAATCAATGGGCAGCAACGAGCTG-3' 5'-CGTGGCACCAGAGCGTTATTAACCTTTTCGGCAGACTCAG-3' |
| GacS _{HH1ND} | 220-654 | 5'-TACTTCCAATCAATGGGCAGCAACGAGCTG-3' 5'-TATCCACCTTTACTGTTATTAGTCGCTGCGCGTCGGGCGGAC-3' |
| GacS _{D1} | 658-793 | 5'-TACTTCCAATCAATGGCCATGGTTTCCGGACGGCC-3' 5'-TATCCACCTTTACTGTTATTACAGCGACTGGCCCAGGCTCAGTC-3' |
| GacS ₁₉₀₋₉₂₅ | | 5'-TACTTCCAATCAATGAGCCGCGCGATCAACGCGCCG-3' 5'-TATCCACCTTTACTGTTATTATCAGAGTTCGCTGGAGTC-3' |
| GacS ₂₅₂₋₉₂₅ | 252-925 | 5'-TACTTCCAATCAATGGCCACCGAGGACGTACGG-3' 5'-TATCCACCTTTACTGTTATTATCAGAGTTCGCTGGAGTC-3' |
| GacS ₂₈₀₋₉₂₅ | 280-925 | 5'-TACTTCCAATCAATGGCGAGCAGGATCAAGTCC-3' 5'-TATCCACCTTTACTGTTATTATCAGAGTTCGCTGGAGTC-3' |
| RetS _{H1} | 409-649 | 5'-TACTTCCAATCAATGACCGCGGAATTGCAGACCAAGGCC-3' 5'-TATCCACCTTTACTGTTATTAGTCGAGCGGCAGGGTCAG-3' |
| Mutations | | Forward primer |
| | | Reverse primer |
| ΔND | | 5'-AGGAGCCGGGCGCCTCCTGGGCCATGGTTTCCGGACGGCC-3' 5'-GGCCGTCCGAAACCATGGCCCAGGAGGCGCCCGGCTCCT-3' |
| Δ76 (EAF + Δ190-269) | | 5'-ATGGAAGCTTTCGAGCTGGACCTGGCGCGCAAGGAG-3' 5'-CCAGGTCCAGCTCGAAAGCTTCCATGCGCAGGGCGAGGAGGGC-3' |
| GacS _{Chimera} | | 5'-AGGATATTCGAACAGTTTTACAGGGTGGATTCTTCGTTG-3' 5'-CAACGAAGAATCCACCCTGTA AAACTGTTTCGAATATCCT-3' |

Table S2. X-ray data collection and structure refinement, related to Figure 1.

| Crystal | GacS _{HH1} | D1apo | D1-BeF3 |
|---|-------------------------------|--------------------------|-------------------------|
| Crystal parameters | | | |
| Space group | P21 | C2221 | C2221 |
| Cell parameters a, b, c (Å) β (°) | a=63.7 b=76.8 c=178.6, β=97.3 | a=69.15 b=73.53 c=104.35 | a=69.69 b=74.01 c=93.34 |
| Data quality | | | |
| Beamline | SOLEIL PX1 | SOLEIL PX2 | SOLEIL PX2 |
| Resolution of data (outer shell) (Å) | 50-2.64 (2.71-2.64) | 36.7-1.45 (1.48-1.45) | 46.7-1.87 (1.91-1.87) |
| Unique reflections | 45042 (2252) | 47424 (2300) | 20248 (1224) |
| Rmerge (outer shell) ^a | 0.078 (3.8) | 0.106 (0.807) | 0.119 (0.678) |
| R _{pim} (outer shell) ^b | 0.027 (1.12) | 0.038 (0.37) | 0.035 (0.220) |
| Mean I/σI (outer shell) | 16 (0.7) | 11 (1.8) | 15.6 (3.7) |
| Multiplicity (outer shell) | 13.6 (13.7) | 8 (5.1) | 13.0 (10.3) |
| Completeness (outer shell) (%) | 100.0 (100.0) | 100 (99.1) | 99.7 (95.2) |
| CC1/2 (%) | 0.998 (0.429) | 0.99 (0.63) | 0.998 (0.807) |
| Ellipsoidal truncation^c | | | |
| Ellipsoid resolution (Å) (direction) | 2.93 (0.382a* + 0.919c*) | n/a | n/a |
| | 2.62 (b*) | | |
| | 2.51 (-0.303a* + 0.953c*) | | |
| | 2.64/3.19 | | |
| Best/worst diffraction limits after cutoff | | | |
| No. of unique reflections | 45042 (2252) | | |
| <1/σI> | 18.1(1.4) | | |
| Spherical completeness (%) ^b | 89.0 (49.6) | | |
| Ellipsoidal completeness (%) ^b | 99.9(99.6) | | |
| Refinement | | | |
| Resolution (Å) | 48.8-2.64 | 36.7-1.45 | 44.61-1.87 |
| No. reflections | 45042 | 45083 | 19241 |
| Protein atoms | 9032 | 2110 | 2052 |
| Solvent waters | 183 | 221 | 213 |
| R _{cryst} ^d | 25.9 | 13.1 | 17.1 |
| R _{free} | 26.6 | 15.3 | 21.4 |
| Rmsd 1-2 bonds (Å) | 0.007 | 0.010 | 0.003 |
| Rmsd 1-3 angles (°) | 0.87 | 1.56 | 1.15 |
| Ramachandran | | | |
| Favoured | 97.8 | 96.9 | 98.4 |
| Outliers | 0.35 | 1.2 | 0.4 |
| PDB accession code | 7Z8N | 7QZO | 7QZZ |

^a R_{merge} = $\sum_{hkl} \sum_i |I_{i(hkl)} - \langle I_{hkl} \rangle| / \sum_{hkl} \sum_i I_{i(hkl)}$, where I is an individual reflection measurement and $\langle I \rangle$ is the mean intensity for symmetry-related reflections.

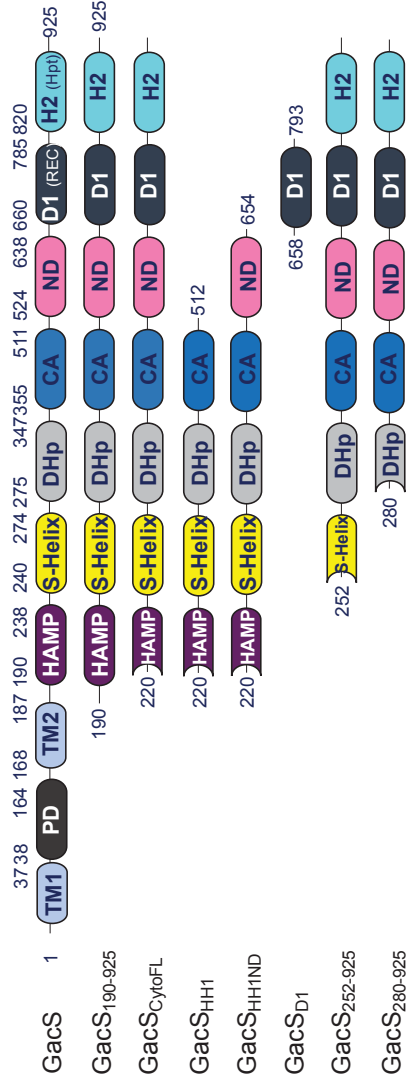
^b R_{pim} = $\sum_{hkl} \sqrt{(1/n-1) \sum_i |I_{i(hkl)} - \langle I_{hkl} \rangle|} / \sum_{hkl} \sum_i I_{i(hkl)}$,

^c Values obtained from staraniso server

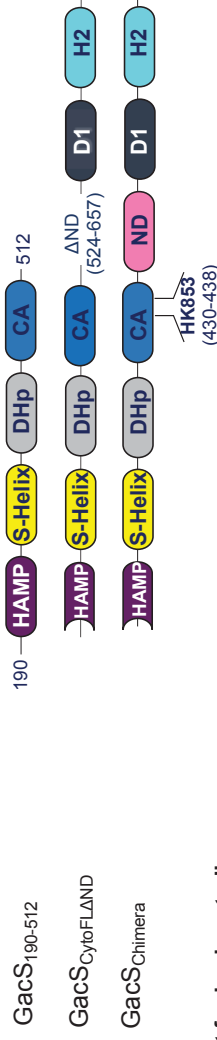
^d R_{cryst} = $\sum_{hkl} | |F_o| - |F_c| | / \sum_{hkl} |F_o|$, where F_o and F_c are observed and calculated structure factors, respectively. R_{free} is calculated for 5% of randomly selected reflections excluded from refinement

Supplementary Figures

A- GacS constructs



GacS Mutants for radioactivity assays



GacS Mutant for in vivo studies



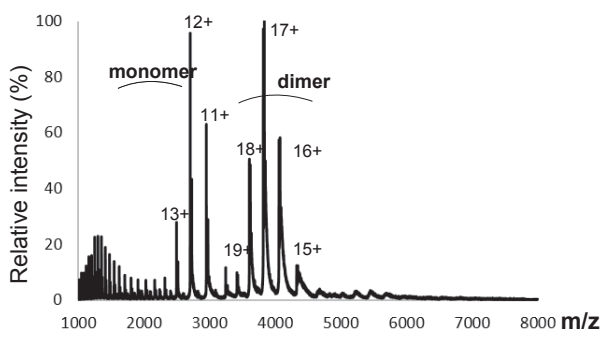
B- RetS constructs



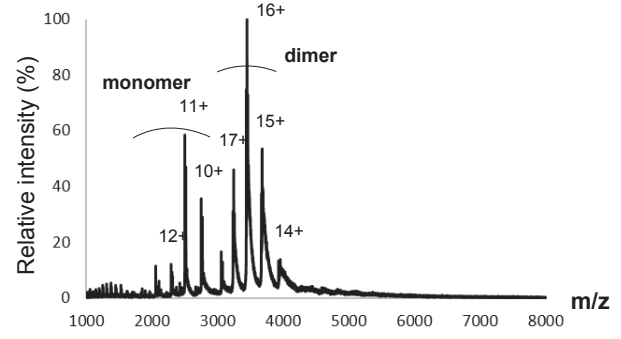
Figure S1. Domain organization of GacS and RetS constructs used in this study, related to Figure 1, 4, 6, 7 and 8 A- Schematic representation of the different GacS constructs used in this study with their boundaries. B- Schematic representation of the different RetS constructs used in this study with their boundaries. Position of punctual mutations within the different domains are indicated. PD stands for periplasmic domain, TM for transmembrane, ND for the uncharacterized domain

1
2
3
4
5
6
7
8
9
10
11
12
13
14
15
16
17
18
19
20
21
22
23
24
25
26
27
28
29
30
31
32
33
34
35
36
37
38
39
40
41
42
43
44
45
46
47
48
49
50
51
52
53
54
55
56
57
58
59
60
61
62
63
64
65

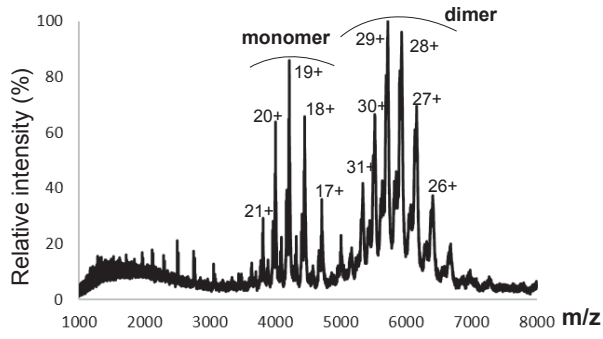
A- GacS_{HH1}



B- RetS_{H1}



C- GacS_{cytoFL}



D- GacS₂₅₂₋₉₂₅

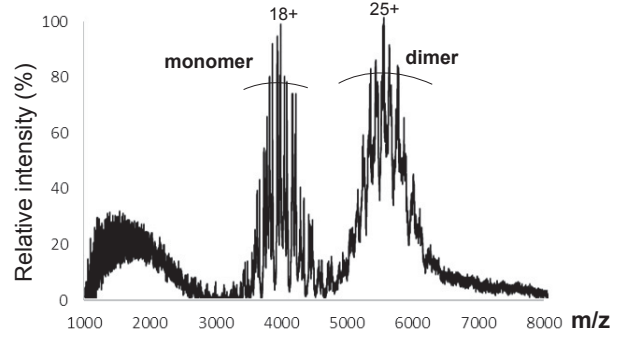
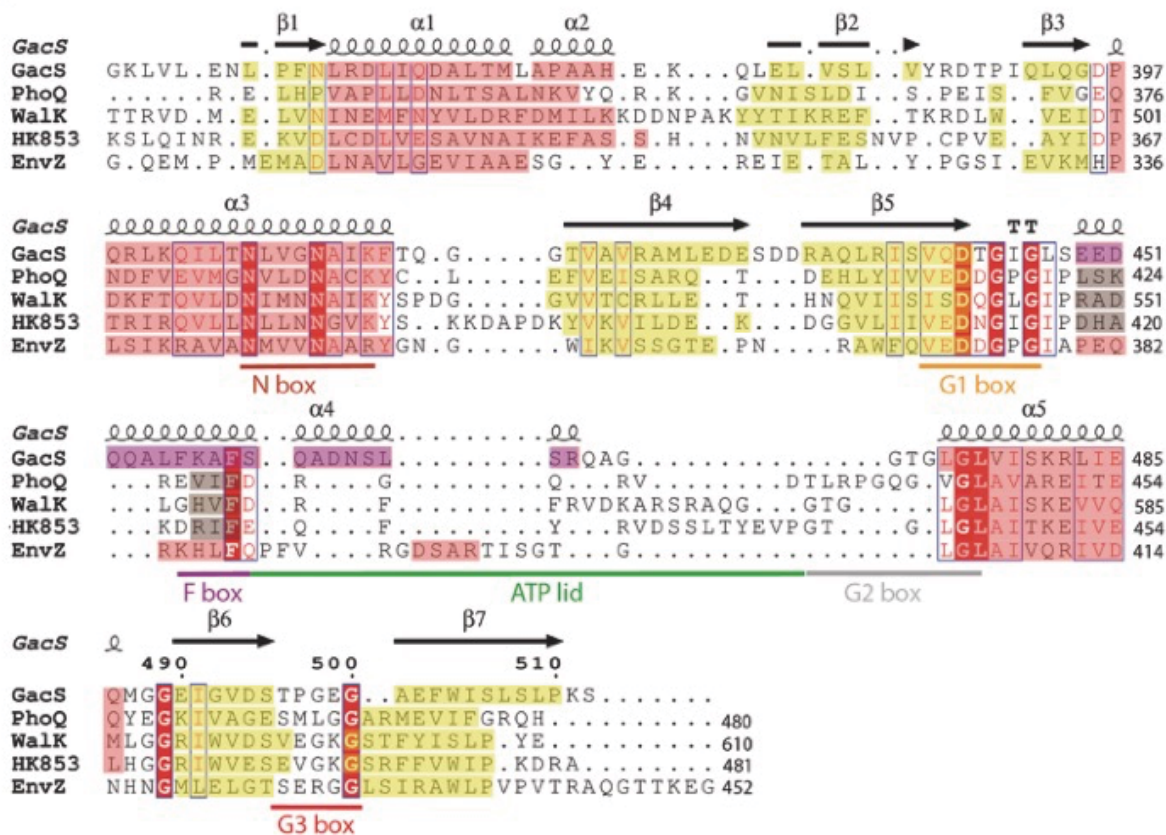
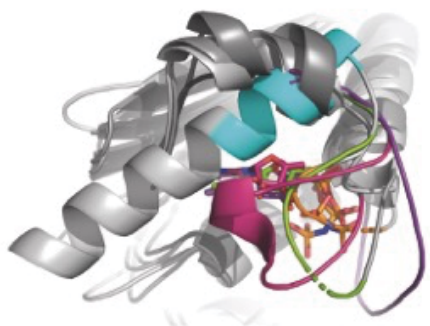


Figure S2. Native mass spectra related to SEC peaks 1, 2, 4 & 6 related to Figure 6 A- GacS_{HH1}, B- RetS_{H1}, C- GacS_{cytoFL} and D- GacS₂₅₂₋₉₂₅. Absolute intensities of monomeric species observed on native mass spectra are overestimated due to a high contribution of the hydrophobic effect. Hydrophobic based interaction can lead to a partial destabilization of dimeric proteins in gas phase as described previously (Bich et al., 2010 ; Southall et al., 2002).

A-



B-



C-

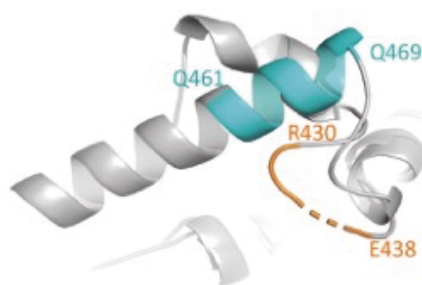


Figure S3. Structural comparison of the ATP lid in bacterial HKs, related to Figure 8. A- structural based sequence alignment of the CA domain from characterized HKs. This alignment has been done with the program Expresso (Armougom et al., 2006). GacS secondary structures are drawn at the top of the alignment and highlighted on the sequence as well as PhoQ (PDB: 1ID0), Walk (PDB: 4U70), HK853 (PDB: 4JAU) and EnvZ (PDB: 4CTI). β -strands are highlighted in yellow α -helices in red, 3_{10} helices in brown and the long helix $\alpha 3$ of GacS is highlighted in purple. B- Structural overlay of HK CA domains. The ATP lid region in the 5 HKs are colored in pink for EnvZ, green for Walk, orange for HK853, purple for PhoQ and cyan for GacS. C- Close up on GacS (cyan) and HK853 (orange) ATP lid regions, boundaries of the interchanged regions are shown with residue numbers.

1
2
3
4
5
6
7
8
9
10
11
12
13
14
15
16
17
18
19
20
21
22
23
24
25
26
27
28
29
30
31
32
33
34
35
36
37
38
39
40
41
42
43
44
45
46
47
48
49
50
51
52
53
54
55
56
57
58
59
60
61
62
63
64
65

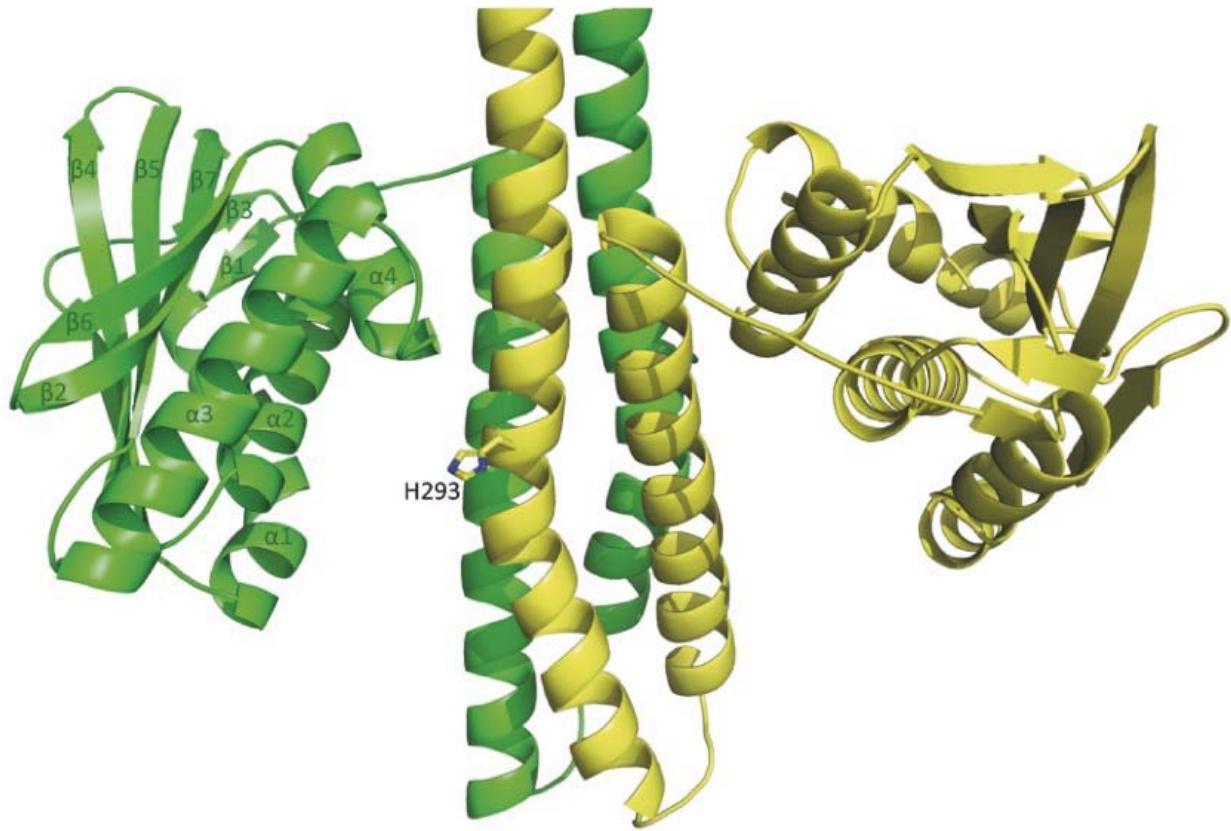


Figure S4. Close-up view of the DHP and CA domains, related to Figure 1. Secondary structure elements on the CA domain are labelled on the green monomer. The phosphorylatable H293 is shown in stick.

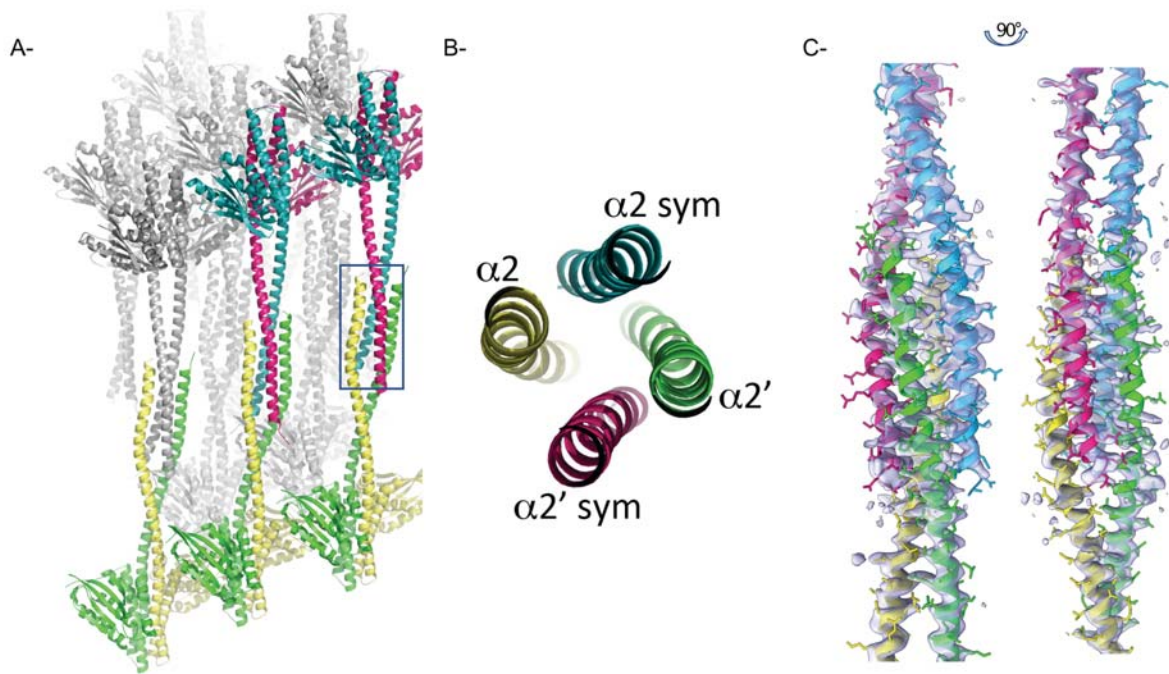


Figure S5- Crystal packing and electron density map, related to Figure 1 A- Crystal packing of the two head-to-tail GacS_{HH1} dimers present in the asymmetric unit with one pair colored in yellow and green and the other blue and pink, the HAMP- α 2 region is framed in blue. B- Close-up view of the HAMP- α 2 region of GacS_{HH1} that stabilize each other by forming a four “bundle like” structure. C- Two 90° representative sigmaA-weighted 2mFo-DFc maps (1 sigma contour level, 0.109e/A³) at a 2.64 Å resolution in the region of the HAMP/S-helix tetramerization site. The final coordinates of the structure are shown with a ball-and-stick model/ribbon schematic representation.

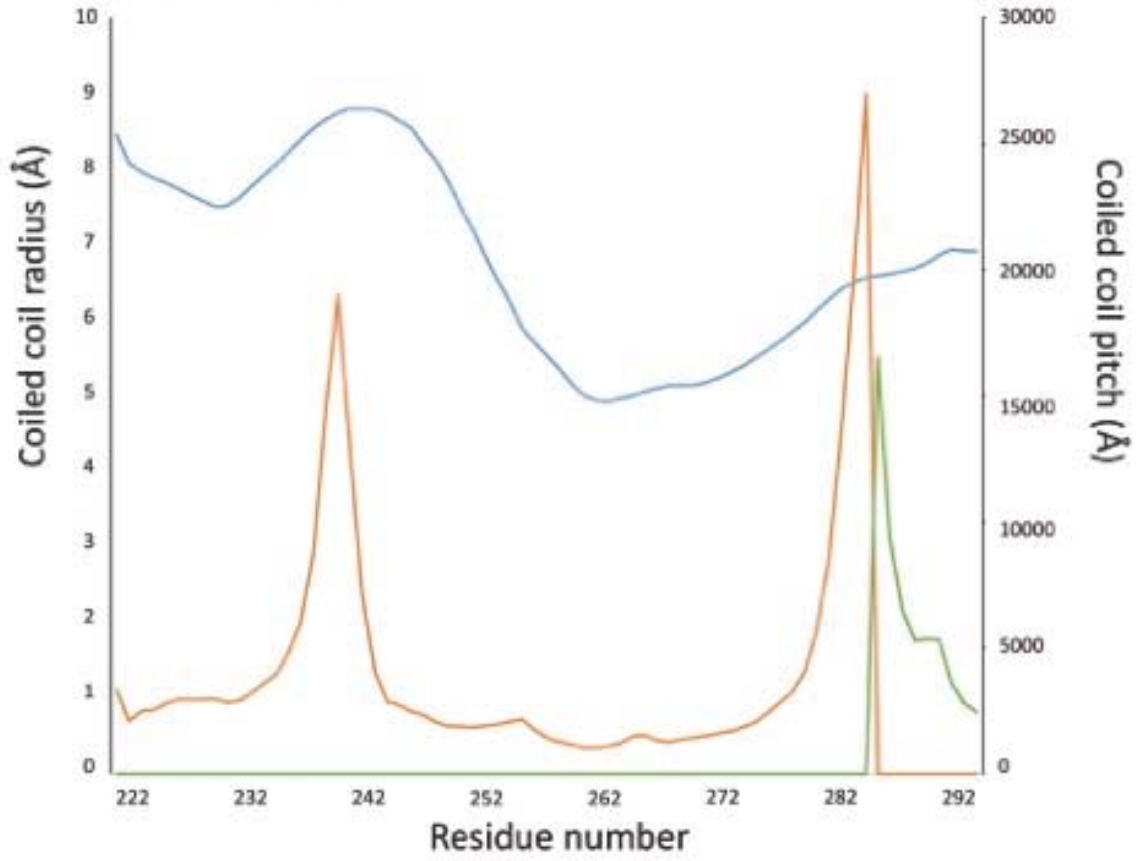
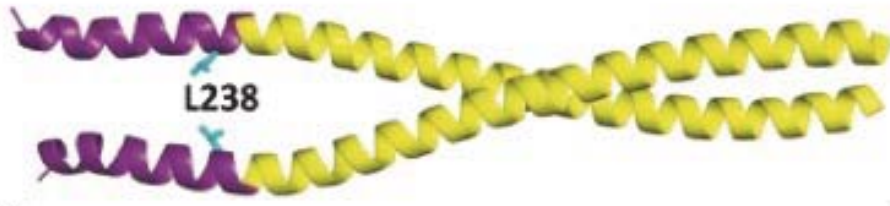
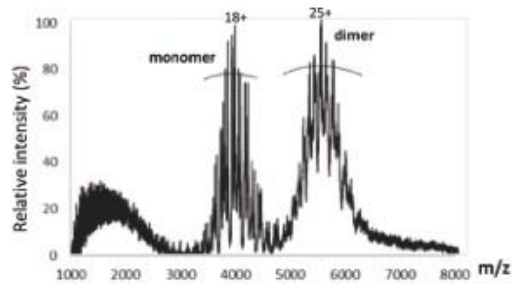


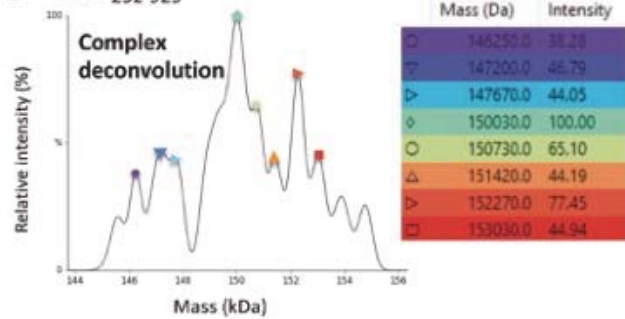
Figure S6. Twister analysis, related to Figure 2. The coiled-coil structure showing the position of the a/d stutter, L238 at the hinge between the HAMP domain (purple) and the S-helix (yellow) (Top). Coiled-coil radius (blue curve) and pitch (orange and green curves) are plotted against residue numbers from the HAMP/S-helix region (Bottom).

1
2
3
4
5
6
7
8
9
10
11
12
13
14
15
16
17
18
19
20
21
22
23
24
25
26
27
28
29
30
31
32
33
34
35
36
37
38
39
40
41
42
43
44
45
46
47
48
49
50
51
52
53
54
55
56
57
58
59
60
61
62
63
64
65

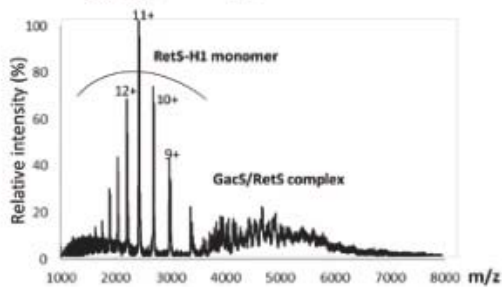
A- GacS₂₅₂₋₉₂₅



C- GacS₂₅₂₋₉₂₅



B- GacS₂₅₂₋₉₂₅+RetS_{H1}



D- GacS₂₅₂₋₉₂₅+RetS_{H1}

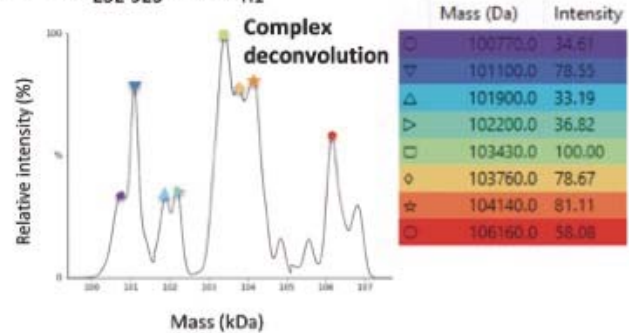


Figure S7: Native mass spectra and deconvoluted mass spectra, related to Figure 6. Native mass spectra related to SEC peaks 6 & 7 of figure 6 (A- homodimer GacS₂₅₂₋₉₂₅, B- complex GacS₂₅₂₋₉₂₅:RetS_{H1}) and related deconvoluted mass spectra. For the peak 6, experimental masses between 146250 and 153030 Da (C) are consistent with the presence of a homodimer of GacS₂₅₂₋₉₂₅ (theoretical mass: 147 521 Da) and for the peak 7, experimental masses between 100 770 and 106 160 Da (D) are consistent with the presence of a complex GacS₂₅₂₋₉₂₅:RetS_{H1} (theoretical mass: 101 276 Da). Native mass spectra have been deconvoluted using Unidec software (Marty et al., 2015).

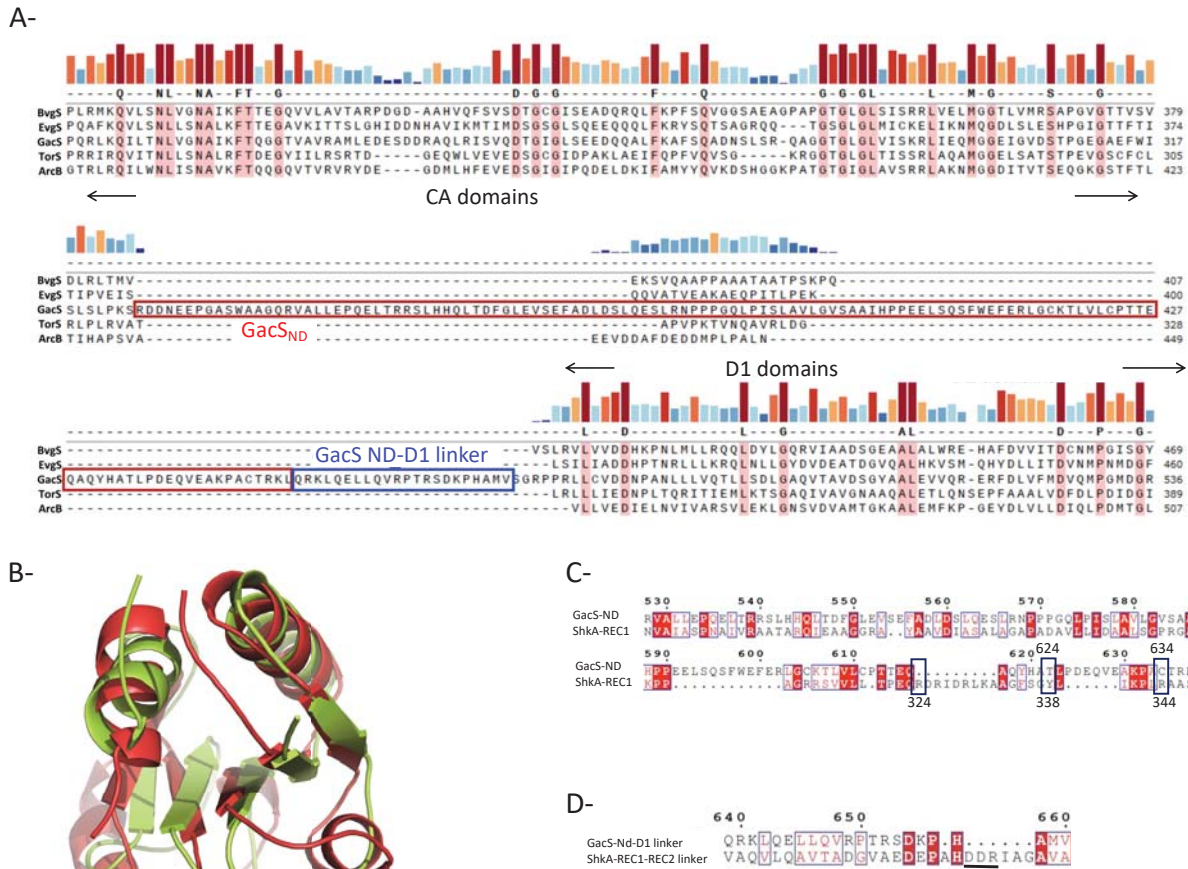


Figure S8. Identification of GacS_{ND} sequence boundaries, related to Figure 8. A- Sequence alignment of GacS with other unorthodox HKs from *Bordetella pertussis* such as BvgS, and from *Escherichia Coli* ArcB, TorS and EvgS, reveals an additional 150-residue cytoplasmic domain (524 to 638) denoted ND. GacS ND domain is framed in red and the linker region is framed in blue. B- The superimposition of the equivalent ND domains structures, RcsC-ABL (in green) and ShkA-PRD (in red). C- GacS-ND aligned with ShkA-REC1 domain. The residues that bind c-di-GMP in ShkA (R324, Y338 and R344), not conserved in GacS, are shown in blue boxes D- GacS ND-D1 linker aligned with ShkA REC1-REC2 linker. The DDR motif in ShkA, not conserved in GacS, is underlined in black.

1
2
3
4
5
6
7
8
9
10
11
12
13
14
15
16
17
18
19
20
21
22
23
24
25
26
27
28
29
30
31
32
33
34
35
36
37
38
39
40
41
42
43
44
45
46
47
48
49
50
51
52
53
54
55
56
57
58
59
60
61
62
63
64
65

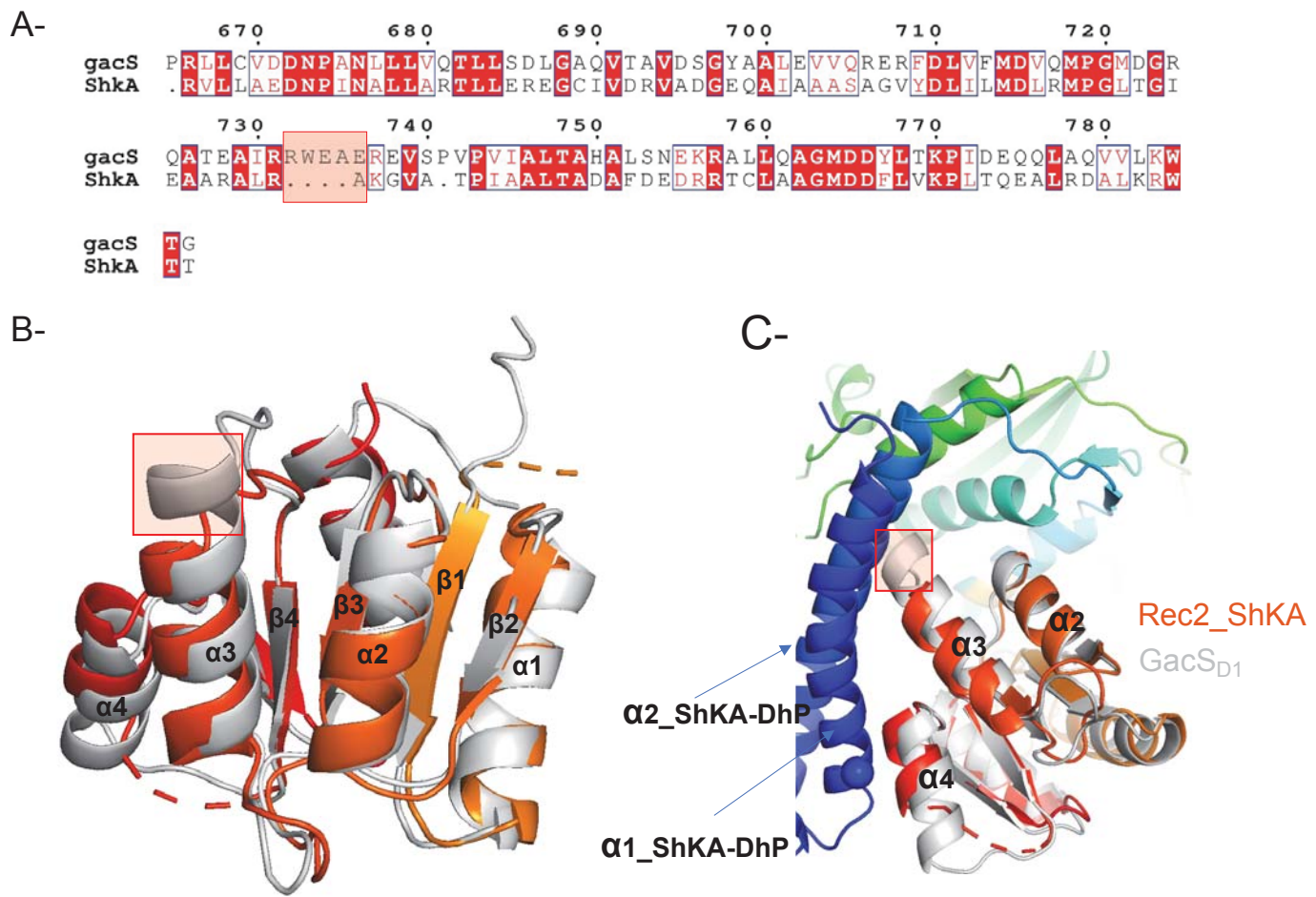


Figure S9. Comparison between ShkA-Rec2 and GacS_{D1} domains, related to Figure 1. A- sequence alignment of GacS_{D1} and ShkA-Rec2, the insertion in GacS sequence is framed in red. B- GacS_{D1} (white) and ShkA-Rec2 (orange) structures are superimposed. Secondary structures labels are common to both structures. The tip of GacS helix $\alpha 3$ is framed in red. C- Superimposition of GacS_{D1} with ShkA-H1-Rec2 structure. The tip of GacS helix $\alpha 3$ is framed in red.